Gonzalo Seco-Granados,
José A. López-Salcedo,
David Jiménez-Baños,
and Gustavo López-Risueño

Unveiling its core features in signal processing

Challenges in Indoor Global Navigation Satellite Systems

Accurately determining one's position has been a recurrent problem in history [1]. It even precedes the first deep-sea navigation attempts of ancient civilizations and reaches the present time with the issue of legal mandates for the location identification of emergency calls in cellular networks and the emergence of location-based services. The science and technology for positioning and navigation has experienced a dramatic evolution [2]. The observation of celestial bodies for navigation purposes has been replaced today by the use of electromagnetic waveforms emitted from reference sources [3].

There is a large variety of radio-navigation systems, ranging from legacy ones dating from the middle of the last century, such as Decca or Loran, to the ones relying on the transmissions from wireless local area network (WLAN) base stations or from the devices found in wireless sensor networks. However, the systems based on satellite transmissions are the ones that play a prominent role today. They are gathered under global navigation satellite systems (GNSS). This term refers to all systems (some of them operational, and others under development) that provide users with positioning information

Digital Object Identifier 10.1109/MSP.2011.943410
Date of publication: 17 February 2012

1053-5888/12/$31.00©2012IEEE

anytime and anywhere around the Earth based on signals radiated from satellites. Thanks to their global coverage, excellent accuracy, and lack of infrastructure requirements for the user, today GNSS is the standard and essential tool for navigation, with applications in key sectors such as transportation (fleet management, en route navigation), civil engineering (surveying and monitoring of infrastructures), precision agriculture (yield mapping, monitoring of chemical distributions), or time reference, just to mention a few. Moreover, the combination of GNSS with other local positioning systems and, above all, with communication systems is spawning new applications, usually found under the umbrella of the topic called location-aware or location-based services (LBSs).

TODAY GNSS IS THE STANDARD AND ESSENTIAL TOOL FOR NAVIGATION, WITH APPLICATIONS IN KEY SECTORS SUCH AS TRANSPORTATION CIVIL ENGINEERING, PRECISION AGRICULTURE, OR TIME REFERENCE.

From a very simplified perspective, the necessary operations in a receiver of a radio-navigation system and, in particular, in a GNSS receiver, can be cast as a set of signal processing problems in detection (to determine which transmitters are received), in estimation (to accurately measure and track the parameters of the received signals), and in optimization (to obtain the position from the equations that link the position coordinates with the signal parameters). Unlike the case with communication receivers and in spite of being a very rich topic in signal processing problems, the use of GNSS signals and the design of GNSS receivers has not been widely addressed by the signal processing community. With some notable exceptions (see e.g., the special issue [4]), most research related to GNSS has stayed in the realm of applied physics and mathematics, and geodesy.

In recent years, two trends have been observed. On one hand, there is an increased interest among the signal processing community in positioning problems [5]–[7]. On the other hand, the success of GNSS in many applications has triggered the demand for making GNSS receivers operational indoors. However, GNSS have been designed to function in outdoor scenarios, and hence their use indoors poses important challenges. We believe that these problems can be attractive to signal processing engineers and researchers, and that our community can provide innovative solutions for many of them.

The goal of this article is twofold. The first half aims at presenting the foundations of GNSS, devoting special attention to the signal and receiver aspects. This will help the reader to have an overview of the current status of GNSS and the modernization plans from the receiver-side perspective. The second half of the article has the objective of presenting in detail the main signal processing problems faced by the use of GNSS indoors and showing some exemplary solutions. In short, our overall goal is to point out topics in sophisticated implementations of GNSS receivers where there is room for new technical contributions, and therefore to stimulate further research onto this topic within our community.

OVERVIEW OF GNSS

GENESIS OF GNSS SYSTEMS

The development of GNSS systems started in the early 1960s, with the U.S. Navy's navigation satellite system, also known as Transit. Originally intended to help the navigation of U.S. submarines, Transit soon became widely adopted by commercial marine navigators. However, and most importantly, Transit paved the way for the launch of subsequent systems (such as Timation and the 621B project) that were called to be the precursors of the current global positioning system (GPS) [8].

GPS was developed by the U.S. Department of Defense (DoD) during the 1970s, although it took over 20 years to make it operational and even longer to fully realize its implications. The result of such a long but profitable period of perseverance is the only fully operational GNSS system today. In parallel with GPS, the Soviet Union started the development of its own GNSS system, GLONASS. Even though its deployment started at roughly the same time as GPS, GLONASS fell into disrepair with the collapse of the Soviet Union in 1991, leaving the system useless for navigation purposes. In recent years, the Russian government committed to restore and maintain the system, but full operation and global coverage is not expected until 2012. Similarly to the American and Russian iniciatives, Europe approved in 2002 the development of Galileo, a European GNSS system under civilian control that is expected to provide high-accuracy global coverage and guaranteed performance. There are currently two experimental satellites in orbit, and the first two operational satellites were just launched in October 2011.

APOGEE OF GNSS SYSTEMS

The resounding success of navigation applications has led the GNSS market to experience double-digit growth rates during the last two decades [9]. This fact, and the need of governments to control their own critical infrastructures, has attracted the interest of other countries such as Japan, China, and India in developing their own global or regional navigation systems. The success of GNSS still continues, now reaching the arena of small portable devices, with a market of more than 500 million GNSS-enabled mobile phones and 100 million personal navigation devices in 2011. One of the key drivers behind this exponentially growing trend was, without any doubt, the issue of the U.S. Federal Communications Commission (FCC) E911 mandate in 1996. This mandate, followed later by the European E112 recommendation, demands mobile terminals to report their position with an accuracy of 50 m for 67% of the time, and 150 m for 95% of the time. Such a requirement, which was independent of the terminal location (both indoors and outdoors), immediately became a technical and economical challenge. Moreover, and particularly in Europe, other economic reasons were also pushing toward the deployment of LBSs. With the E911/E112 infrastructure in place, LBSs are seen by carriers

as a way to increase their average return per user (ARPU) and thus recoup some of their high third-generation (3G) licensing costs [10].

DURING THE LAST DECADE, SIGNIFICANT EFFORTS HAVE BEEN CARRIED OUT TO DEVELOP TECHNIQUES AND TECHNOLOGIES MAKING MOBILE PHONES CAPABLE OF DETERMINING THEIR POSITION.

NEED FOR INDOOR GNSS RECEIVERS

During the last decade, significant efforts have been carried out to develop techniques and technologies making mobile phones capable of determining their position. An excellent survey of the several wireless positioning techniques can be found in [11]. Some of them rely on local infrastructure and therefore have local coverage. The techniques that have wide coverage are essentially those based on the cellular networks and those employing GNSS. The former group is commonly referred to as network-based positioning and consists of techniques such as observed time difference of arrival (OTDOA) and uplink time difference of arrival (UTDOA), in second-generation (2G) and 3G networks, respectively. A comprehensive review of these techniques was presented in a previous special issue of *IEEE Signal Processing Magazine* [5]. As for the latter group, the use of GNSS signals, which provide good performance in open sky environments, solves the accuracy problems of network-based positioning in rural or scarcely populated areas. The use of GNSS in this context has received the name of assisted GNSS (AGNSS), and it is currently incorporated as part of the 3GPP Release 7 [12]. The main idea behind AGNSS consists of using the communication capabilities of wireless networks for disseminating assistance data to GNSS-enabled mobile terminals [13]. This assistance allows a reduction in the required computational burden and the time-to-first-fix (TTFF), while improving the positioning accuracy of GNSS receivers. Nevertheless, many challenges do appear when moving AGNSS receivers indoors due the severe signal degradation. This is a critical aspect, particularly when nearly 80% of mobile calls either originate or terminate inside buildings. This situation sparked the research interest in indoor GNSS, and led to the development of advanced signal processing techniques for GNSS signals, originating the concept of high-sensitivity GNSS receivers (HS-GNSS).

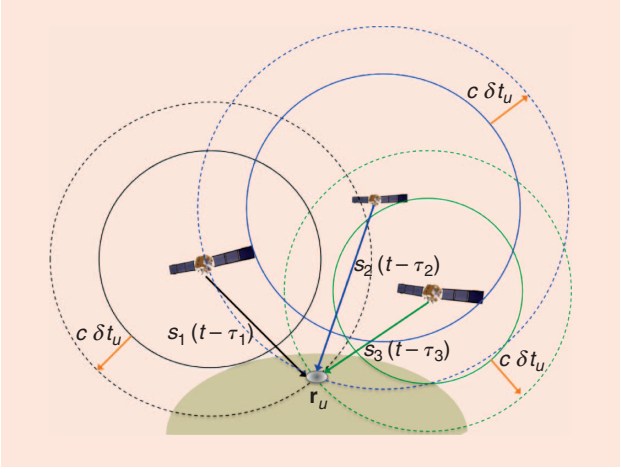

[FIG1] Illustration of the rationale behind GNSS positioning and the effect of unknown receiver clock offset.

FOUNDATIONS OF GNSS POSITIONING

Before entering into the problematics of indoor GNSS, it is important to introduce the very basic concepts that make GNSS positioning possible in its standard outdoor operation. The basis of GNSS positioning is the computation of range estimates obtained by means of the so-called time-of-arrival (TOA) measurements. That is, the user's position is determined by measuring the signal propagation delay between each visible satellite and the receiver. It is for this reason that time-delay estimation becomes a topic of paramount importance in GNSS receivers.

First, let us present conceptually how a GNSS receiver determines the different ranges. Each satellite transmits at least one signal with a time stamp associated with it, which we denote as $t_{s,i}$ for the ith satellite. At the user's side, the receiver measures the time of reception of the transmitted stamp, $t_{u,i}$, and it obtains an estimate of the propagation delay for the ith satellite as $\tau_i \doteq t_{u,i} - t_{s,i}$. Then the distance between the satellite and the user can be calculated as $d_i = c\tau_i$, with c being the speed of light.

In practice, a GNSS receiver measures the transmit time of the signal and just reads the reception time from an internal clock [14, Ch. 5]. The transmit time is obtained by observing the specific portion of the signal (recall that the signal is time stamped) that is received at the very same instant where the receiver is reading its internal clock. The determination of the received portion of signal boils down to aligning the incoming signal with a local replica of the transmit signal, which is essentially known at the receiver except for some amplitude changes, and it is therefore a synchronization problem.

As a first approximation, we can assume that the position of each satellite is known in advance. The satellite position can be computed using some coefficients known as ephemerides, which are transmitted by the satellite itself. Thus, the estimated distance provides the radius of the spherical surface centered at the satellite and containing the user's location. Actually, this would be true if the transmit and receive times were measured in the same time scale, but this is not the case. All satellites from the same system ideally share the same time scale, which is referred herein as the GNSS time. This is due to the control exerted by the ground control segment, but this time scale is not available at the receiver since it is run by an independent clock. Therefore, all range measurements d_i are shifted by an unknown term, expressed as $c\,\delta t_u$, where δt_u represents the offset between the receiver time and the GNSS time. Note that the time scale may indeed be different from one GNSS system to another [15]. That's why the term "GNSS time" does not refer herein to a common time scale to

all GNSS systems but just to the particular time scale of the GNSS system under analysis (e.g., either GPS or Galileo).

We consider momentarily the case of two-dimensional positioning for the sake of simplicity. The spherical surfaces become circumferences, which are shown in Figure 1, including the effect of the unknown clock offset. The variables to be determined by the intersection of the circumferences are the position coordinates and δt_u. It can be seen in the figure that the intersecting points of any pair of circumferences change for different values of δt_u. However, the key concept underlying GNSS positioning is that the three circumferences share a unique intersection point for an appropriate value of δt_u. Rigorously, the intersection need not be unique, but in practical terms a single intersecting point is considered because the other possible intersections occur at places (e.g., thousands of kilometers away from the Earth) where the user is sure not to be. This means that, in a two-dimensional problem, measurements to at least three satellites are needed to determine the user's position. Applying the same type of arguments, one can justify that a minimum number of four satellites is needed to compute a three-dimensional (3-D) position. Note that the value of δt_u is necessarily found as a by-product of the positioning process, which means that besides obtaining the position the receiver can be synchronized to the GNSS time scale.

Unfortunately, the measurements d_i are affected by several disturbing effects. As in any receiver, the measurements are degraded by interference and noise, but there are some effects that are specific of GNSS such as time-delay errors caused by clock biases at the satellites, tropospheric and ionospheric delays, errors in the satellite ephemerides, relativistic effects, or variations of the propagation delay caused by multipath propagation, to mention only the more common ones. In general, the various sources of error can be categorized in three main groups, depending on whether they have the origin in the satellite and control segments, the propagation of the signal, or the local effects at the receiver. The error budget for outdoor GNSS positioning can be found in any reference book on GNSS, such as in [8, Ch. 11] and [16, Ch. 7]. The ionosphere and the multipath are usually considered to be limiting factors in the accuracy achievable with GNSS. However, the relative importance of the different error sources radically changes in an indoor scenario, where thermal noise (including interference if present) is by far the greatest problem due to the large line-of-sight (LOS) signal attenuation. Unlike what happens in outdoor scenarios, ionospheric errors, which can reach the order of tens of meters, have secondary relevance because they are exceeded by the errors induced by the thermal noise. Multipath propagation is a very deleterious factor indoors, and additional effects such as the near-far appear as well (a detailed description of these effects is provided in the section "Challenging Problems in the Reception of GNSS Signals Indoors"). The most widespread error mitigation strategies in GNSS consist of using differential techniques and measurements at several frequency bands. These strategies are valid to combat errors from the first two categories mentioned above, but they do not offer any protection in front of locally generated effects (noise, interference, and multipath), which are precisely the limiting factors in indoor GNSS. This means that the abundance of error-mitigation techniques existing in GNSS is of reduced interest for an indoor receiver, and this explains the great importance of using more sophisticated signal processing techniques, since they are virtually the only way to improve the performance of GNSS indoors (let alone of the integration with other systems).

SOPHISTICATED SIGNAL PROCESSING ALGORITHMS ARE EVEN MORE NECESSARY WHEN ONE INTENDS TO EXTEND THE USE OF GNSS BEYOND THE LIMITS OF THEIR ORIGINAL DESIGNS.

The receiver actually obtains a range measurement that can be modeled as

$$d_i = \rho_i + c(\delta t_u - \delta t_{s,i} + \delta t_{\epsilon,i} + \delta t_{\text{iono},i} + \delta t_{\text{tropo},i} + \delta t_{\text{rel},i} + \delta t_{n,i}) \tag{1}$$

where ρ_i is the true geometric distance between the ith satellite and the receiver, $\delta t_{s,i}$ is the clock bias, $\delta t_{\epsilon,i}$ is the bias incurred due to errors in the ephemerides, $\delta t_{\text{iono},i}$ is the ionospheric delay, $\delta t_{\text{tropo},i}$ is the tropospheric delay, $\delta t_{\text{rel},i}$ is the relativistic error, and $\delta t_{n,i}$ represents the contribution of both multipath and noise terms. Note that the selection of error terms in (1) is only an example that includes the most common terms considered in the literature, but it does not intend to be exhaustive and it does not imply that all the terms in that expression are relevant in all cases. The subindex i is added to all terms that are satellite dependent. Since the distance measurements d_i are shifted by the unknown quantity $c\delta t_u$, they are referred to as a pseudoranges.

The process leading to an estimate of the user's position, $\mathbf{r}_u \doteq [x_u, y_u, z_u]^T$, is called navigation solution. There are essentially two families of navigation solutions, and recently mixed solutions have been proposed [17]. In the first one, the position is obtained in closed form. The best known representative is the Bancroft algorithm [18]. These techniques provide worse accuracy than those in the second family, which corresponds to iterative solutions based on the linearization with respect to $\mathbf{r}_u$. For the sake of illustrating the principles underlying the iterative solutions, we present the simplest one, which is based on the least-squares fitting between the measurements and the model. For this purpose, we can rewrite (1) as

$$\widetilde{d}_i = \rho_i + c\delta t_u, \tag{2}$$

where $\widetilde{d}_i$, denoted as corrected pseudorange, is computed by subtracting from d_i any possibly available estimates of the right-hand side terms of (1). The effects that need to be modeled explicitly depend on the accuracy sought for the position. Residual errors and terms that cannot be estimated, such as

$\delta t_{n,i}$, are left unmodeled (i.e., removed from the equation). Next, the geometric distance is linearized around a tentative value of the user's position, $\mathbf{r}_{u,0} \doteq [x_{u,0}, y_{u,0}, z_{u,0}]^T$, by keeping the first-order term of the Taylor series

$$\rho_i(\mathbf{r}_{s,i}, \mathbf{r}_u) = \|\mathbf{r}_{s,i} - \mathbf{r}_u\| \approx \|\mathbf{r}_{s,i} - \mathbf{r}_{u,0}\| - \frac{(\mathbf{r}_{s,i} - \mathbf{r}_{u,0})^T}{\|\mathbf{r}_{s,i} - \mathbf{r}_{u,0}\|} \Delta\mathbf{r}_u, \quad (3)$$

where we have made explicit the dependence of ρ_i on $\mathbf{r}_{s,i}$ and $\mathbf{r}_u$, and $\Delta\mathbf{r}_u = \mathbf{r}_u - \mathbf{r}_{u,0}$. Using this approximation and stacking all of (2) together, for N_{sat} satellites, we obtain the following matrix equation:

$$\mathbf{y} = \mathbf{H}\Delta\mathbf{u}, \quad (4)$$

where $\mathbf{y} = [\,\widetilde{d}_1 - \|\mathbf{r}_{s,1} - \mathbf{r}_{u,0}\|, \ldots, \widetilde{d}_{N_{\text{sat}}} - \|\mathbf{r}_{s,\rho_{N_{\text{sat}}}} - \mathbf{r}_{u,0}\|\,]^T$, $\Delta\mathbf{u} = [\Delta\mathbf{r}_u, c\delta t_u]$, and $\mathbf{H}$ is an $N_{\text{sat}} \times 4$ matrix whose ith row is $[-((r_{s,i} - r_{u,0})^T/\|r_{s,i} - r_{u,0}\|), 1]$. It is evident that at least $N_{\text{sat}} = 4$ satellites are needed to solve (4). If there are more than four satellites, the system is overdetermined and the standard least-squares solution can be used

$$\Delta\mathbf{u} = (\mathbf{H}^T\mathbf{H})^{-1}\mathbf{H}^T\mathbf{y}. \quad (5)$$

Actually, it is customary to use a weighted least-squares solution, where the weight of each equation is somehow related to the quality of the corresponding measurement. The user's position is updated using (5), and the process can be iterated taking the resulting position as the new tentative value around which the equations are linearized again. In practice, two iterations are normally sufficient to reach the solution of the original nonlinear problem even if the first tentative position has an error on the order of kilometers.

GNSS SIGNAL CONSIDERATIONS

SIGNAL MODEL FOR GNSS-TRANSMITTED SIGNALS

The description in this section focuses on the GPS signal. The reasons are twofold. First, GPS is the system currently used by the majority of commercial satellite positioning devices. Second, most features of GPS signals are shared by other GNSS systems, and hence the discussion in the following subsections is applicable for them as well.

The signal transmitted by the ith satellite can be expressed as

$$s_{c,i}(t) = \sum_{l=-\infty}^{\infty} d_l \sum_{k=0}^{N_r-1} u_k c_{c,i}(t - kT_{\text{code}} - lT_d), \quad (6)$$

where $d_l = \{-1, +1\}$ are the data symbols (or bits) transmitted at a rate of $R_d \doteq 1/T_d = 50$ bits per second (bps), constituting the navigation message; $c_{c,i}(t)$ is the unique composite pulse (also known as the primary code or simply the code) used by the ith satellite. The subscript $_c$ denotes a continuous-time signal to avoid confusion with its discrete-time counterpart. This composite pulse has a time duration (i.e., code period) of $T_{\text{code}} = 1$ ms and it is repeated $N_r = 20$ times within each bit interval, which means that $u_k = 1$ for all k. Instead of repeating the primary code within the bit period, a longer spreading sequence can be built in a tiered manner by modulating each of the N_r primary codes using amplitudes $u_k = \{-1, +1\}$, as done for instance in Galileo. In that case, u_k denotes the kth chip of a so-called secondary code with length N_r.

Actually, $s_{c,i}(t)$ is a direct-sequence spread-spectrum (DS-SS) signal with the composite pulse being formed as $c_{c,i}(t) = \sum_{j=0}^{N_c-1} v_{j,i} p_c(t - jT_c)$, where $p_c(t)$ is a bandlimited rectangular pulse and $v_{j,i} = \{-1, +1\}$ are the pseudo-noise (PN) chips with duration T_c that form the signature of the ith satellite, with $N_c = 1{,}023$. The chip rate is $R_c \doteq 1/T_c = N_c/T_{\text{code}} = 1{,}023$ megachips per second (Mc/s).

Each GPS satellite transmits several signals of the same type as (6). For instance, the one already described would correspond to the so-called coarse-acquisition (C/A) signal, which is the one used by all GPS commercial receivers. A similar signal to the one in (6) is transmitted by GPS satellites in the quadrature component using the so-called precision (P) code. The code actually being transmitted is indeed an encrypted version of the P code known as the P(Y) code, having a chip rate of $R_c = 10.23$ MHz and a code period slightly longer than 38 weeks. The result is a ranging signal with a very large spreading gain providing outstanding immunity to noise and jamming signals. Such a formidable performance is not publicly available since the P(Y) code is reserved for military applications only. In any case, the common practice in military receivers is to first acquire the freely available C/A code (thus the name "coarse-acquisition") and then process the P(Y) code.

For simplicity reasons, we will henceforth omit any subindexes indicating the satellite and the component signal inside the satellite. By omitting these subindexes, we just have to keep in mind that $s_c(t)$ represents a generic signal among the large number of signals with similar characteristics simultaneously being transmitted by one satellite of the GNSS system.

SIGNAL MODEL FOR GNSS-RECEIVED SIGNALS

A receiver located outdoors with LOS conditions would receive the following continuous-time complex baseband equivalent signal,

$$x_c(t) = A_0 \cdot s_c((1 + F_{d,0}/F_x)t - \tau_{c,0})e^{j2\pi F_{d,0}t} + w_c(t), \quad (7)$$

where A_0, $\tau_{c,0}$, and $F_{d,0}$ are the complex amplitude, delay, and Doppler frequency of the received signal, F_x denotes the carrier frequency, and $w_c(t)$ includes the contribution of the thermal noise, signals from the same or other satellites, replicas of $s_c(t)$ due to multipath propagation, and any other interference. Cross-correlation interference with other GNSS signals is almost negligible outdoors. This is because the adopted PN codes provide more than 20 dBs of interference protection, which is large enough to absorb the few dBs of power variations among different satellites outdoors. It is important to remark that F_d is called the Doppler frequency for convenience. It

incorporates not only the contribution due to the relative movement between the satellite and the user's receiver, but also the frequency shift due to the instability of the receiver clock with respect to its nominal value. For the former, typical values are within ± 5 kHz for a land vehicle, and twice this value for high-speed aircrafts [19]. Note also that the narrow-bandwidth approximation has not been applied in (7) and hence, the effect of the Doppler shift has been taken into account in the complex envelope of $x_c(t)$. As we will see later on, the time expansion or contraction of the signal, as observed from the receiver, cannot be discarded to obtain accurate measurements and it becomes even more crucial in indoor receivers.

The quality of the GNSS-received signal is typically measured in terms of the so-called carrier-to-noise spectral density, $C/N_0 \doteq |A_0|^2/2N_0$, contrary to the widely adopted signal-to-noise ratio (SNR) in communication systems. This is mainly because C/N_0 is a bandwidth-independent measure, and thus, it allows to easily compare different GNSS receivers regardless of their bandwidths. Note that in GNSS, the receiver bandwidth is selected depending on the required accuracy and the allowed receiver complexity, whereas in communication systems, it is fixed and determined by the symbol rate and the modulation scheme. Typical values of $C/N_0 \geq 44$ dB-Hz are commonly found in outdoor GNSS working conditions.

Finally, it is important to mention that probably all GNSS receiver implementations are based on digital architectures where the input signal is digitized at the very early stages of the receiver chain. In this case, the discrete-time representation of the signal in (7) becomes

$$x(n) = A_0 \cdot s((1 + f_{d,0}/f_x)n - \tau_0)e^{j2\pi f_{d,0}n} + w(n), \qquad (8)$$

where $x(n) \doteq x_c(nT_s)$, $s(n) \doteq s_c(nT_s)$, and $w(n) \doteq w_c(nT_s)$, with T_s the sampling period. As for the synchronization parameters, $\tau_0 \doteq \tau_{c,0}T_s$ and $f_{d,0} \doteq F_{d,0}T_s$ represent the discrete-time delay and the discrete-time frequency shift, while $f_x \doteq F_xT_s$ stands for the discrete-time carrier frequency. Note that T_s will be dropped hereafter for the sake of clarity. We define the variable N_{scode} as the number of samples in one code period, i.e., $N_{\text{scode}} \doteq T_{\text{code}}/T_s$, as it will be used repeatedly later on.

MAIN DIFFERENCES BETWEEN GPS AND OTHER SYSTEMS

From a physical layer perspective, existing GNSS systems can be classified into two main categories. On one hand, those GNSS systems which are based on code division multiple access (CDMA) such as GPS, Galileo, and the modernized version of GPS, also known as GPS-III. On the other hand, we have the GLONASS system adopting a frequency division multiple access (FDMA) instead. For the first group of systems, the following distinctive features can be highlighted with respect to conventional GPS:

- A pilot signal is conveyed into the quadrature component of Galileo signals (E1, E5a, E5b, E6) and modernized GPS signals (L1C, L2C, L5) to improve the signal acquisition and tracking.
- Longer spreading codes, also known as primary codes, are adopted. For instance, in the Galileo E1 and the modernized GPS-L1C and L2C signals, $N_c = 10{,}230$ chips. For the latter signal, this code length is only adopted in the in-phase component, since the quadrature component carries a different code with an even longer length of $N_c = 767{,}250$ chips.
- Higher chip rates are also adopted, with $R_c = 5.115$ Mc/s in Galileo-E6 or $R_c = 10.23$ Mc/s in Galileo-E5 and GPS-L5. For the GPS-L2C signals, however, a slightly lower chip rate of $R_c = 511.5$ kilochips per second is adopted.
- Tiered codes are formed by concatenating N_r primary codes, which are amplitude sign-modulated according to the values u_k of the so-called secondary code.
- Channel coding is introduced to protect the navigation message, typically a rate 1/2 convolutional code with constraint length seven for Galileo and modernized GPS-L2C and L5 signals. LDPC codes are used in the modernized GPS-L1C signal.
- Nominally, the received power is slightly higher. For instance, in the L1 band, around 1 and 1.5 dB more power will be received with Galileo and modernized GPS, respectively.
- New modulation formats are introduced based on the concept of binary-offset-carrier (BOC), which can be understood as a signal with rectangular pulses (as in traditional GPS) multiplied by a train of narrower rectangular pulses with alternated sign. A time-multiplexed BOC (TMBOC) is adopted in the modernized GPS L1C signals [20] and a composite BOC (CBOC) in Galileo E1 [21]. They both are compliant with the multiplexed BOC (MBOC) power spectral density agreed by the United States and European Union for the GPS-III and Galileo compatibility. An alternated BOC (AltBOC) signal is adopted in Galileo E5 consisting of four trickily multiplexed codes that provide a constant envelope signal.

The new features presented above will have an effect on the performance and on the implementation of the receiver algorithms, but not on the fundamental operating principles of each system, which essentially remain the same. Something similar can be said about the GLONASS system, which despite being based on an FDMA scheme, transmits a spreading sequence in each carrier frequency. Thus, for each subband, a CDMA signal has to be acquired at the receiver anyway. The code length of this sequence is $N_c = 511$ chips for the C/A component and $N_c = 5.11 \cdot 10^6$ chips for the P component. The chip rate is $R_c = 0.511$ Mc/s and $R_c = 5.11$ Mc/s, respectively.

GNSS SIGNAL PROCESSING AND RECEIVER ARCHITECTURE

The ultimate goal of any GNSS receiver is to determine the user's position based on the analysis of a set of received signals coming from the satellites in view. The procedure to be followed, far from being straightforward, consists of several tasks to be carried out in a sequential manner. The block diagram for a standard GNSS receiver is illustrated in Figure 2. In (a), the front-end module is just a generic block that carries out the

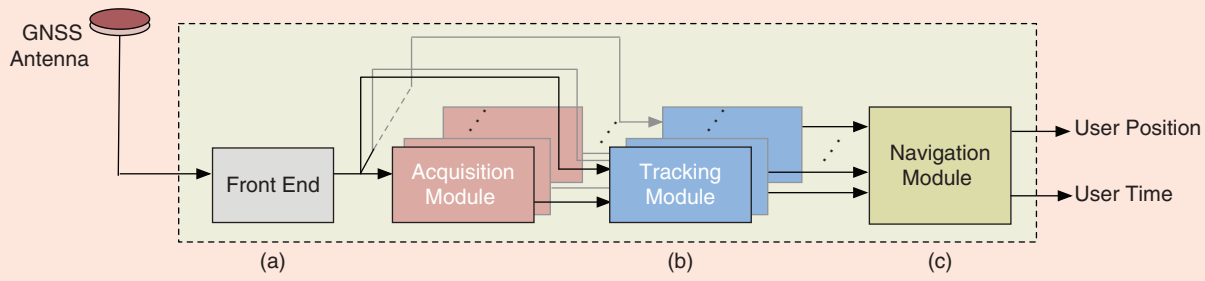

[FIG2] **Parts (a)–(c) show the general architecture of a standard GNSS receiver.**

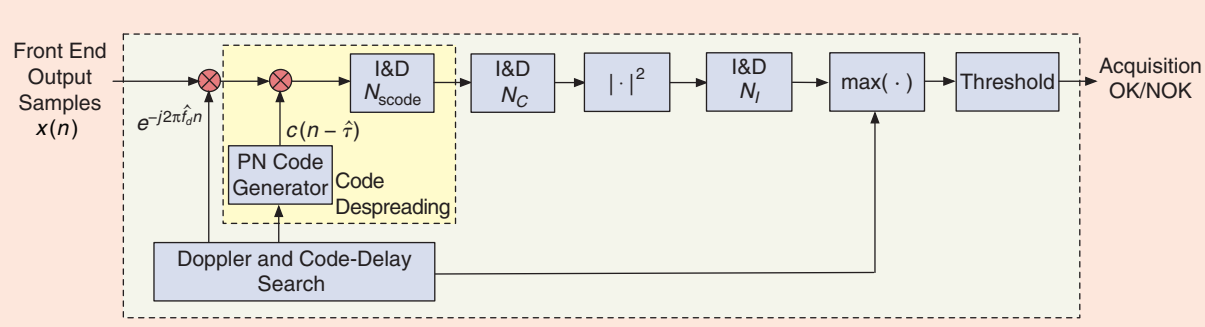

[FIG3] **Acquisition architecture for a GNSS receiver where the integration time has been extended in a noncoherent manner.**

signal conditioning in a similar way as it occurs in a communication receiver (i.e., bandpass filtering, low-noise amplification, baseband conversion, and analog-to-digital conversion). In (c), the navigation module is in charge of solving the user's position following the conceptual procedure already presented in the section "Foundations of GNSS Positioning." In (b), a set of specific signal processing modules are required, and these are indeed the focus of this section.

ACQUISITION

Once the input signal has been properly conditioned, the first task a GNSS receiver must perform is detecting the satellites currently in view. These satellites will serve as the anchor points from which the user's position will be determined, a mission to be accomplished by measuring the time it takes for the transmitted signal to reach the user's receiver. The obtention of this time-delay estimate, or at least the provision of a rough initial guess, is the primary goal of the acquisition stage. However, there are some unwanted effects that further complicate this process. The most relevant one is the presence of a Doppler shift in the received signal, which forces the acquisition stage to perform a two-dimensional (time-frequency) search. This is done by correlating the received signal with a locally generated replica with tentative code-delay and Doppler shift values. Note that such a correlation consists in multiplying the input signal with the local replica, and then adding together the N_{scode} samples in a code period to wipe off the code and despread the signal. This process is carried out within the code despreading module indicated in Figure 3, and it is repeated for all the possible values of code-delay and Doppler shift. The signal is then declared to be acquired when the magnitude of the obtained correlation exceeds the signal detection threshold. The acquisition code-delay and Doppler shift estimates become those tentative values where the magnitude of the signal correlation exhibits the highest peak, depicted in its time-frequency representation in Figure 4. The minimum coherent integration (CI) time within these correlations is thus N_{scode} samples (i.e., one code period) but it can be extended in a coherent manner by adding together up to N_C code periods, as indicated in the acquisition architecture depicted in Figure 3. In this figure, integrations are indicated in the form of integrate-and-dump (I&D) blocks, which also

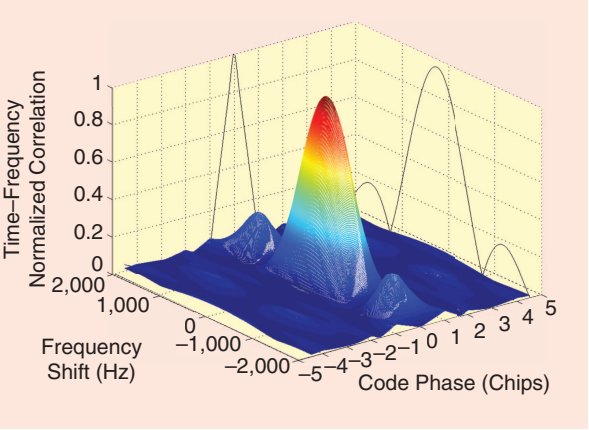

[FIG4] **Time-frequency representation of the correlation peak to be acquired.**

reduce the output rate compared to the input rate in the factor indicated inside the block.

In most outdoor working conditions, the basic CI of just one code period (i.e., $N_C = 1$) is enough for detecting the presence of the current satellite being searched. This involves just 1 ms CI for the case of GPS-L1 C/A signals. Problems arise when moving indoors, since the severe attenuation makes it very difficult to detect the received signals. Such a sensitivity problem can be compensated provided that a sufficiently long integration time can be used, so that the noise can be filtered out. Unfortunately, this statement, which is theoretically valid, cannot be applied in practice because of the presence of two main limitations that prevent increasing N_C without bound:

1) The received signal is data modulated and there is a risk of signal cancellation if a bit transition occurs while coherently integrating the signal. The average losses due to bit transitions are $L_c(\text{dB}) = -10\log_{10}(1-(N_C N_{\text{scode}})/(3N_{\text{sbit}}))$, with N_{sbit} the number of samples per bit period. These losses cannot be avoided since the navigation data bits are still unknown at this stage of the receiver.

2) The received signal is affected by residual frequency errors and there is a risk of signal cancellation when CI exceeds a given time duration. Such a cancellation can be understood by analyzing the SNR gain when integrating N_C samples under a frequency error F_ϵ. The gain is given by $\Delta\,\text{SNR}(\text{dB}) = 20\log_{10}|\sin(\pi F_\epsilon T_{\text{code}} N_C)/(\sin(\pi F_\epsilon T_s)| - 10\log_{10} N_C$ and is depicted in Figure 5. As it can be observed in this figure, the smaller the residual frequency shift, the longer the CI can be made before the SNR gain collapses due to phase wrapping. This effect suggests a tradeoff between SNR gain and computational burden, due to the fact that reducing the residual frequency shift involves performing a finer Doppler search, thus requiring more operations to be carried out.

The increase in computational burden is not the only limitation of implementing a long CI. Beyond a given point, the presence of phase noise due to the oscillator instabilities may also cause the coherently accumulated phase to collapse anyway. It is for this reason that, for practical purposes, the CI time cannot increase without bound. In these circumstances there is no choice but to resort to the combination of coherent and non-CIs (NCIs) to further extend the overall integration time and improve the receiver sensitivity. This process is shown in Figure 3, where the CI output is squared and followed by an I&D of N_I samples to extend the total integration time to $N_C N_I$ code periods. The SNR gain is shown in Figure 5.

TRACKING

From the signal processing standpoint, GNSS receivers are essentially extremely accurate synchronizers. The accuracy requirements are much more demanding than in communication receivers dealing with similar bandwidths, since GNSS timing errors are scaled by c (which is a very large number) when converted into ranging errors. It is for this reason that the

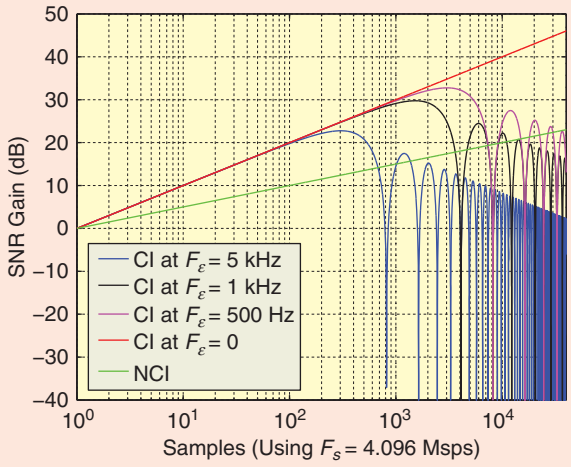

[FIG5] ΔSNR for CI with different frequency errors and for NCI.

coarse code-delay and Doppler estimates obtained at the acquisition stage must be refined and tracked to accurately follow any possible time variation. Such a continuous monitoring of the synchronization parameters is performed by the so-called tracking stage. Two parallel closed-loop architectures are implemented for this purpose, which are referred to as the delayed-lock loop (DLL) for the code tracking, and the phased-lock loop (PLL) for the carrier tracking. Both architectures are shown in the tracking module depicted in Figure 6. As it can be seen, they are indeed the same architectures that can be found in a continuous-transmission (not burst mode) spread-spectrum communication receiver.

Being closed-loop schemes, the goal of the DLL and the PLL is to obtain fine estimates of the code-delay and Doppler shift parameters, respectively, by comparing the input signal with the locally generated replica and driving the resulting error signal to zero. For the case of the DLL, the signal replica is just the output of a PN generator that is driven by a numerically controlled oscillator (NCO). For the PLL, the signal replica is indeed a complex (in-phase/quadrature component) carrier generator which is also driven by a carrier NCO. In both cases, once the signal replica is correlated with the input signal, the result is fed to a discriminator that will output a signal roughly proportional (on average) to the error in the parameter to be tracked. As shown in Figure 6, three correlations are indeed employed for code tracking: one computed at the prompt or on-time delay, and the other two located symmetrically before and after the prompt one, which are called early and late correlations. This configuration leads to the family of early-late methods, where the discriminator output is one way or another formed by comparing the early and late correlations [16, Ch. 5]. The discriminator output is then smoothed with a loop filter before driving the corresponding NCO, thus closing the loop. This a priori, rather simple architecture has been widely analyzed in past decades, with several contributions regarding the loop filter design [22], coherent and noncoherent

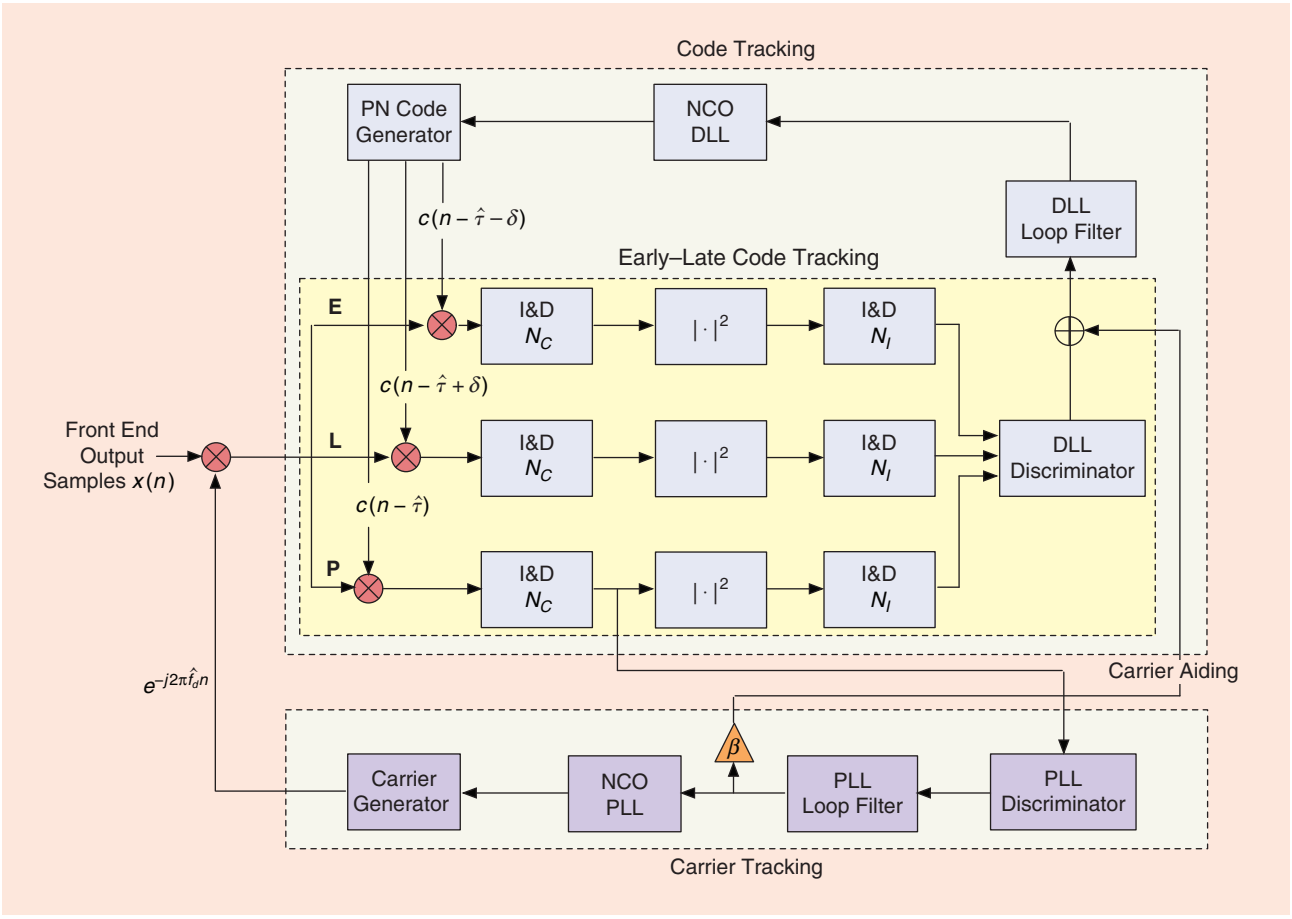

[FIG6] **General architecture of the tracking module of a traditional GNSS receiver.**

discriminators [16, Ch. 5], and closed-loop performance analyses [8, Ch. 7], [23]–[24].

DATA DEMODULATION

When both code and carrier are properly wiped off from the received signal, the receiver is ready to recover the navigation data bits from where to extract the satellite ephemerides, clock correction parameters, the ionospheric model, some health/status messages, and time stamps on the received signal. To do so, frame synchronization is firstly required to determine the starting point of the words, subframes, and pages of the navigation message. Once achieved, information can be retrieved in a straightforward manner for the case of GPS, where no coding scheme is adopted but just a parity check. For the case of modernized GPS and Galileo, convolutional or LDPC encoding is incorporated and data decoding is required.

Among the set of parameters that can be extracted from the navigation message, the time stamps on the received signal are certainly of paramount importance. They are constituted by a certain known sequence of bits embedded into the navigation message, and they allow the receiver to know the exact time at which any point of the signal has been transmitted. In the case of GPS, the signal is marked every 6 s using the so-called time-of-week (TOW) field within the handover word (HOW), and the system time scale is known as the GPS time. Decoding the HOW is therefore required to know the GPS time reference. If for any reason this is not possible, the time stamps will not be available and the time-of-arrival of the received signal cannot be directly obtained from the signal (workarounds for this problem are presented in the section "Synthetic Recovery of the Signal Time Stamps").

CHALLENGING PROBLEMS IN THE RECEPTION OF GNSS SIGNALS INDOORS

Originally designed for outdoor clear-sky operation, GNSS receivers are found to fail when moving to indoor environments. The reason lies in the degradation effects experienced by the signal when propagating through the so-called satellite-to-indoor channel. That is, degradations due to propagation through building elements such as the roof, external and internal walls, floors, or any other indoor obstacle such as moving persons or furniture. The effects can be summarized into two main parameters [25]: the building entry loss, which accounts for the losses due to propagation through the building materials; and the delay/angle spreading, which accounts for the reflection, refraction, and scattering that cause a single incident ray to be received as an ensemble of clusters of phase-shifted, time-delayed, and attenuated paths. From a more practical

perspective, entry losses and time-delay/angular spreadings can be understood in terms of three simple and intuitive degradations, which are also commonly found in traditional wireless communications systems: signal attenuation, multipath, and near-far effects.

SIGNAL ATTENUATION

The very first degradation that indoor GNSS receivers have to cope with is the severe signal attenuation due to the propagation through building materials. External building obstacles such as the roof or the façade may introduce up to 30 dB of attenuation to the refracted signal penetrating indoors. In addition to this, a GNSS receiver placed in an inner room may be affected by some extra dB of attenuation due to walls, furniture, the floor, or any other internal obstacle. Table 1 presents some indicative attenuation values at the GPS-L1/Galileo-E1 frequency band for some of the most common building materials [26].

A myriad of possible working conditions can be found in practice when operating a GNSS receiver indoors. However, just some simple calculations are needed to understand the challenge of making a GNSS receiver operate indoors. Let us recall that the nominal outdoor working conditions are typically $C/N_0 \geq 44$ dB-Hz. For an indoor scenario, and depending on the building materials and the receiver location within the building, attenuation losses ranging from ten to more than 30 dB can be experienced, as indicated in Table 2.

In these circumstances, the first question to be asked is whether these severely attenuated signals can be reliably detected. The answer can be found by using a well-known result from statistical detection theory, which states that 3 dB are gained each time the CI interval is doubled, whereas for non-CI, only 1.5 dB are asymptotically gained [27]. According to this result, the number of CIs, N_C, would need to be increased in a factor of 10^3 to recover the 30 dB of attenuation introduced by the indoor environment. In terms of non-CIs, N_I, the situation is even worse, requiring the integration time to increase by a factor of 10^6. These numbers provide an idea of the cost, in terms of acquisition time, that the detection of indoor GNSS signals involves compared to the nominal outdoor working conditions. In practice, a combination of both coherent and non-CIs is adopted, leading to different acquisition sensitivities, as shown in Figure 7.

For the case of time-delay estimation, an indication of the achievable performance is provided by the Crámer-Rao bound (CRB). For GPS-L1 C/A signals in a deep indoor scenario (e.g., $C/N_0 = 10$ dB-Hz) the root mean square error of time-delay estimates may be on the order of 30 m [28]. Depending on the satellite geometry and assuming all visible satellites to have $C/N_0 = 10$ dB-Hz (which is a very pessimistic assumption), this time-delay error may turn into positioning errors ranging from 60 to 180 m, falling within the tolerance margin imposed by legal mandates on the location of emergency calls. Thus, at least from a theoretical point of view, indoor GNSS positioning seems to be a feasible challenge. However, tighter bounds such as the Ziv-Zakai bound should be considered to realistically determine the GNSS time-delay estimation performance at very low C/N_0 values.

[TABLE 1] ATTENUATION OF DIFFERENT BUILDING MATERIALS AT 1.5 GHZ [26].

MATERIAL	SIGNAL ATTENUATION (dB)
GLASS	1–4
TINTED GLASS	10
WOOD	2–9
ROOFING TILES/BRICKS	5–31
CONCRETE	12–43
REINFORCED CONCRETE	29–33

Regarding data demodulation, an outdoor GNSS receiver typically operates with an energy-per-bit-to-noise spectral density $E_b/N_0 \geq 27$ dB, which already provides a quasi-error free performance. With indoor attenuation values greater than 30 dB, the received E_b/N_0 falls well below the Shannon limit of -1.6 dB and the navigation data bits cannot be recovered anymore. This implies missing the satellite ephemerides and the time stamps on the signal. The lack of the navigation message can be overcome with the AGNSS concept, whereby the navigation message or equivalent information is sent to the GNSS receiver by means of a terrestrial communication system, such as a cellular mobile system or a WLAN. The provision of time stamps via the communication system is more problematic because it requires a very precise synchronization between the three parties involved: the navigation/communication receiver, the communication network, and the GNSS time. Although some of the current networks have the capability of providing this synchronization, it is a feature that is preferably not implemented because of complexity and cost issues at the network side. The computation of the position in the absence of time stamps or synchronization with the network is still possible, but as it will be shown later on in the section "Synthetic Recovery of the Signal Time Stamps," the procedure is more complex than in a conventional receiver.

MULTIPATH

The key assumption in the design of GNSS systems is the presence of perfect LOS between each of the visible satellites and the user's receiver antenna. As it can be seen in Figure 8, this situation is commonly encountered in clear-sky outdoor conditions, but progressively degrades when moving into more problematic environments such as the urban canyon and indoor locations.

[TABLE 2] CLASSIFICATION OF TYPICAL INDOOR WORKING SCENARIOS.

SCENARIO	ATTENUATION LOSSES (DB)	RECEIVED C/N_0 (DB-HZ)	EXAMPLE: THE RECEIVED SIGNAL PENETRATES THROUGH...
SOFT-INDOOR	10–20	35–25	... A NEARBY WINDOW.
INDOOR	20–35	25–10	... A REINFORCED CONCRETE WALL.
DEEP-INDOOR	≤ 35	≤ 10	... A REINFORCED CONCRETE ROOF WITH ASPHALT MEMBRANES.

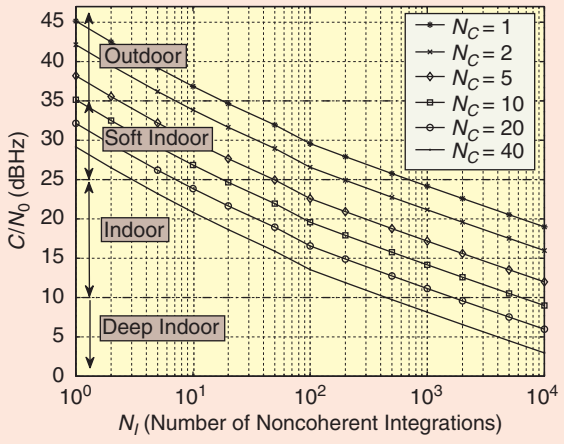

[FIG7] GNSS receiver sensitivity with different combinations of coherent and non-CIs. The values correspond to the acquisition of a given coarse frequency bin with a fine frequency search space of 20 equidistant bins in the range [−500, 500] Hz. The global probability of false alarm is $P_{FA} = 10^{-6}$ and the probability of detection is $P_D = 0.9$. No data bit transitions are assumed during the integration time.

The main source of degradation for GNSS receivers is certainly the presence of either natural or man-made obstacles, causing the transmitted signal to be reflected and refracted in its way to the receiver end. In these circumstances, the received signal is typically composed of phase-shifted, time-delayed, and attenuated signal replicas, forming the so-called multipath contribution. Two types of multipath can be distinguished:

- *Coherent multipath* denotes those reflections (typically specular) that have a time-delay difference (w.r.t. the LOS signal) on the order of or smaller than the inverse of the signal bandwidth and a Doppler difference smaller than the inverse of the coherent correlation interval. Coherent multipath is often neglected in wireless communication systems in virtue of the so-called narrowband fading approximation [29]. In GNSS, however, this type of multipath introduces a systematic error in the time-delay estimation of the aggregate received signal and thus, cannot be neglected in practice [30].
- *Noncoherent multipath* denotes those reflections (typically diffuse) that arrive with a larger time-delay and Doppler shift. These multipath components are usually exploited in wireless communication systems as a source of diversity for improving the overall symbol error rate (e.g., as in RAKE receivers for spread-spectrum systems [31]). In contrast, noncoherent multipath does not play a relevant role in GNSS systems because it does not provide any information on the LOS time-delay, which is indeed the primary parameter of interest in a GNSS receiver.

The impact of multipath depends on several factors such as the relative power compared to the LOS signal, and the time-spread of the overall multipath contribution. These two parameters determine the degree of distortion of the LOS signal, and thus the bias in the estimate of the LOS time-of-arrival. To provide an idea of the order of magnitude of this bias, it can be said that for the case of pseudorange measurements, multipath errors typically range from tens to hundreds of meters. A more dramatic situation occurs when moving to indoor scenarios. In this case the LOS component may even not be present, and the receiver has no choice but to try to acquire the received signal parameters based on a collection of indistinguishable overlapped signal replicas. This situation, illustrated in Figure 9, challenges the basis of satellite-based positioning because there is no reference LOS signal that could provide truthful information on the geometric distance between the satellite and the user's receiver.

In view of these evidences, understanding the underlying behavior of indoor multipath becomes a key element for the success in making GNSS receivers operate indoors. Several studies and measurement campaigns have been conducted with the aim of characterizing the so-called satellite-to-indoor channel [25]. However, most of these works only address specific aspects of the channel, specific environments, or frequency bands other than the navigation L-band where GNSS operates. Some of these works are briefly summarized next.

- The envelope of GNSS-received signals was investigated in [32] confirming that the probability density function can be

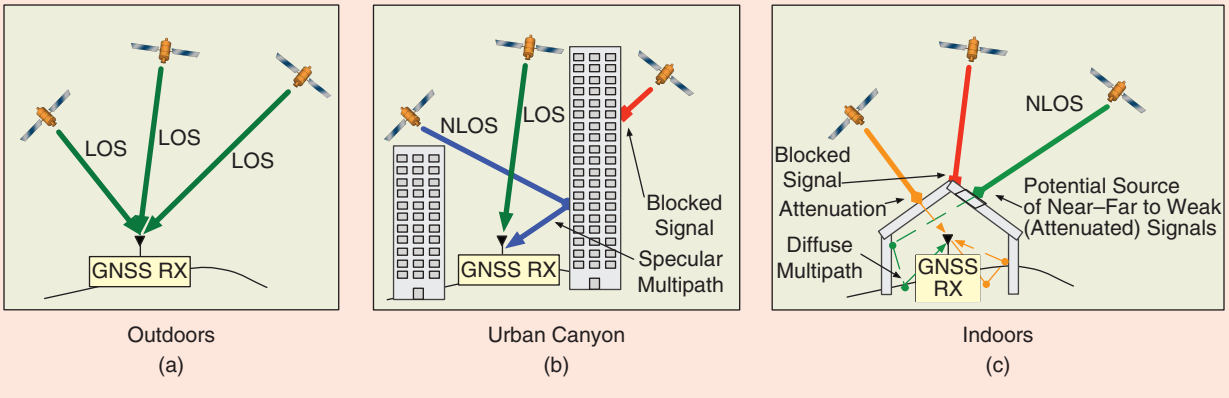

[FIG8] Illustration of the (a) outdoor, (b) urban canyon, and (c) indoor scenarios for a GNSS receiver.

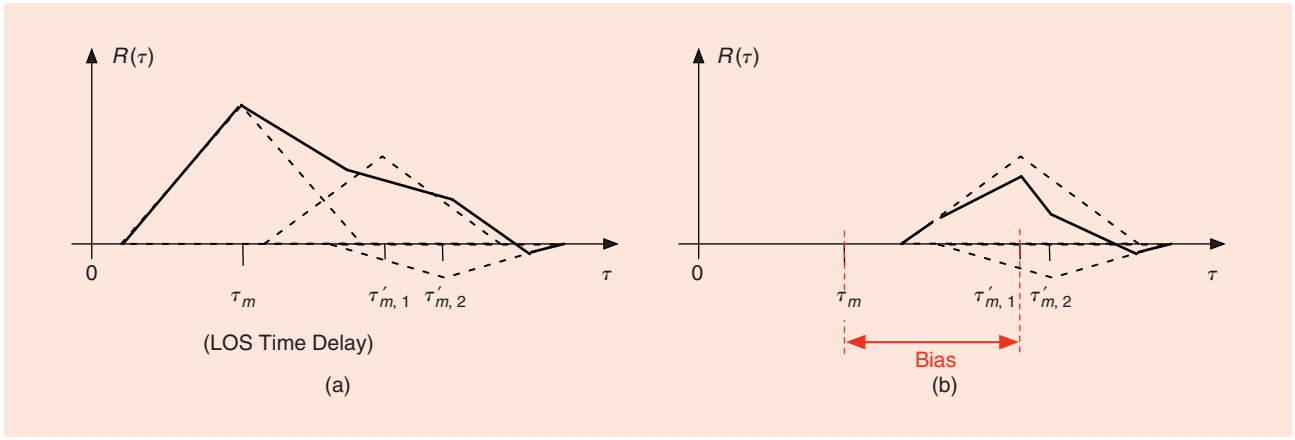

[FIG9] (a) Correlation peak for LOS with multipath and (b) for NLOS. Part (b) shows the bias incurred when the reference LOS signal is not present.

modeled as a combination of: a Rice component with LOS signal-to-multipath ratio (SMR) in the range $[2, 150]$ corresponding to the LOS signal plus short delay multipath components; a Rayleigh component corresponding to multipath rays with power P_m where $P_m^{-1} \in [15, 120]$; and a Loo component corresponding to LOS signals with log-normal attenuation (e.g., due to foliage) plus short delay Rayleigh multipath components with $P_m^{-1} \in [15, 20]$. The ratios of presence of each distribution are in the ranges of $[0.22, 1]$, $[0, 0.78]$, $[0, 0.65]$, respectively, depending on the particular environment.

- A measurement campaign in the S-band channel between a helicopter and the interior of a building is reported in [25] and [33]. Experimental cumulative density functions of the received power are provided. A so-called deterministic model is presented, which consists in performing a ray tracing analysis using the uniform geometrical theory of diffraction. Indoor delay spreads ranging from 25 to 200 ns are reported, corresponding to a fading coherence bandwidth of 5 MHz to 40 MHz, larger than the main lobe bandwidth of GPS-L1 C/A signals but on the order of the bandwidth of Galileo signals.
- Another measurement campaign from a helicopter to the interior of a building was conducted in [34], [75], and [76] but targeted the specific GNSS frequency band, and provided analytical models for the indoor channel rather than empirical distributions. Based on the traditional Saleh-Valenzuela (S-V) multipath channel model, some modifications were added to reflect directional information to take into account the strong dependence of GNSS multipath with the incident angle.
- By using measured and simulated signals, the contributions in [35]–[37] show that the land mobile multipath channel model implemented in Spirent simulators [38] can be used to generate signals whose performance approaches that of real indoor signals with great fidelity. The correlation coefficient between simulated power and code-delays with real values is always greater than 0.9.
- A comprehensive characterization of fading and multipath is presented in [39] for two indoor environments, a tube walkway and the top floor of a four-story building. Experiments were done with an ad hoc-developed software that gathers raw signal samples from a Nokia front end. This is probably one of the best references for a detailed description of the propagation effects in indoor GNSS, encompassing some results and experiments already addressed in previous contributions.

NEAR-FAR

Different attenuation values among the signals coming from different satellites is an additional detrimental effect for indoor GNSS receivers. This power unbalance problem is also experienced in cellular communication systems where it is widely known as the near-far effect. In cellular systems, these power differences are due to the disparate possible distances from mobile terminals to base stations, leading to different propagation losses. On the contrary, all received signals usually hold similar powers in outdoor GNSS. But indoors, severe power variations are experienced because of the different attenuation losses incurred by the different propagation paths; for instance, one satellite signal may come through the window and another may come through the ceiling [as shown Figure 8(c)].

GNSS signals possess an inherent protection against near-far effects that is provided by the use of spreading codes with cross-correlation margins on the order of $24 - 28$ dB (e.g., for GPS-L1 and Galileo-E1 signals). These cross-correlation values assume no bandwidth limitation, and they typically fall down to $20 - 24$ dB, or even less, when small receiver bandwidths are considered (e.g., as in the case of handheld receivers). As it was previously shown in the section "Signal Attenuation," indoor attenuation values may range from just a few dB when propagating through a window, to more than 30 dB when penetrating through concrete walls. In these circumstances the inherent robustness of GNSS signals is not enough to withstand the near-far effect indoors. These effects may lead to the three following situations: weak signals from satellites in view are not detected; weak signals from satellites in view are detected but the measured pseudorange has a huge error; a satellite not in view is declared to be present. The latter situation can be easily solved in AGNSS receivers because the information about the satellites currently in view is embedded

into the broadcasted assistance message.

From the application point of view, near-far detection is much more important than mitigation. If the near-far interference on one signal turns out to be undetected, the error in the pseudorange and, hence, in the position estimate will be extremely large (e.g., tens of kilometers). If the near-far interference is detected but not mitigated, the satellite will be declared unavailable and, unless the receiver does not have enough available satellites, position fixes will be computed. The acknowledgment that the position cannot be calculated at a given time instant is not as damaging as a largely erroneous information.

FROM THE APPLICATION POINT OF VIEW, NEAR-FAR DETECTION IS MUCH MORE IMPORTANT THAN MITIGATION.

TECHNOLOGICAL CONSTRAINTS

The limiting aspects of GNSS-based indoor positioning are not only arising from the propagation environment but also from the application and technological boundary conditions. In particular, there is a clear trend of including GNSS receivers into mobile phones and handheld devices, where the use of low-cost, low-consumption, small size, and lightweight components is of paramount importance. The price to be paid for the use of such components is an unavoidable performance degradation in terms of clock accuracy and computational power that must be circumvented somehow with the design of smarter and more efficient signal processing techniques. Some examples of the current technological challenges to be faced are summarized in the list below.

- Clocks used in handheld devices are typically temperature-controlled crystal oscillators (TCXO) whose main commercial merits are low cost and small size. However, TCXO clocks may compromise GNSS acquisition due to higher long-term frequency instabilities and higher sensitivity to temperature variations, as compared to other much more accurate clocks such as oven-controlled crystal oscillators (OCXO) or atomic clocks. The latter offer the best existing stability, but their adoption in commercial applications is far from becoming reality due to their large cost, size, and power consumption. Nevertheless, some miniaturized prototypes are starting to be announced [40], [41].

  In the meantime, TCXO clocks will continue to be widely adopted in commercial handheld devices. Signal processing efforts have thus to be aimed at coping with the side effects of this technology, which can be classified into deterministic and random frequency fluctuations. The former are related to aging and drifting caused by implementation mismatches. They can be fairly modeled with a second-order polynomial, where the second-order term represents the aging effect. When a priori known, these deviations can be compensated. If not, the GNSS acquisition stage has to account for them by increasing the search space. For typical TCXO clocks with 1 part per million (ppm) of frequency stability, this may imply to explore an additional ± 1.5 kHz range. This is particularly critical for AGNSS receivers that do not perform frequency acquisition, since the accuracy of the assisted Doppler estimates may be completely useless due to the receiver internal frequency deviation. As for the random fluctuations of the clock phase, they are the result of different random disturbances (i.e., white, flicker, and random walk noises) and they cannot be predicted. A widely adopted metric for measuring such a short-term random fluctuation is the Allan variance, $\sigma_A^2(T)$ [42]. It provides the standard deviation of accumulated phase error in T seconds of CI as, $\theta_{3\sigma}(T) = 2\pi F_x T \sigma_{\text{allan}}(T)$ [16, Ch. 4]. This accumulated phase error is an additional impairment that prevents indoor GNSS receivers to implement long CIs, thus limiting the SNR gain before signal detection.
- The number of hardware elements to be implemented in GNSS-enabled mobile devices should be kept to the minimum. This leads to the exploitation of software-defined radio (SDR) architectures, where digitization is moved closer to the receiver antenna and the rest of signal processing is carried out with digital signal processors. Some manufacturers are currently offering navigation receivers in which the signal processing is entirely executed in the processor already present in the handheld device (typically an ARM processor). The main advantage of this approach is that it provides a high level of flexibility for reconfiguring the signal processing algorithms via firmware updates, a suitable choice for enabling compatibility with future GNSS signals and further enhancements to high-sensitivity receivers [43]. The price to be paid is a huge increase in the computational load for the digital processor, longer latency times, and higher power consumption.
- In the race toward reducing power consumption in GNSS-enabled mobile devices, the industry target is set below 100 milli Joules (**mJ**) per position fix, leaving GPS monitoring to a background task with no noticeable user impact on battery life [44]. It is thus mandatory to implement all the signal processing algorithms in the most power-efficient manner. An illustrative example is the extensive adoption of FFT processors for implementing the correlation between the received signal and local code replicas [19]. However, one of the main drawbacks of FFTs is their block-processing architecture, which poses many difficulties when just a reduced subset of correlation bins wants to be calculated [45]. This situation appears, for instance, when the signal being tracked is lost briefly (e.g., when driving under an overpass). Instead of starting the whole acquisition process from scratch again, it makes sense to reuse previous knowledge on the received signal with the aim of reducing the search space and speeding up the obtention of a new position fix. A similar situation appears for the so-called snapshot or push-to-fix receivers (i.e., acquisition-only receivers) typically adopted indoors, where long integrations are required. In these type of receivers no tracking is implemented and position fixes are provided under demand [46]. Both in the case of outdoor

reacquisition and snapshot indoor receivers, there is no need to compute the full correlation of the incoming signal with the local replica as the nominal FFT does. Alternatives for the calculation of just a few correlation lags are being explored with the use of zoom, pruning, and fractional FFT methodologies [47].

IT IS CLEAR THAT TO BE EVENTUALLY ABLE TO DETECT WEAK SIGNALS, THERE IS NO CHOICE BUT TO ACCUMULATE THE SIGNAL ENERGY DURING LONG OBSERVATION INTERVALS.

- Another important issue for GNSS positioning is the time-to-fix (TTF), which represents the time that a GNSS receiver requires to provide a position fix. TTFs smaller than 10 s are being sought, forcing indoor GNSS receivers to rely on the AGNSS concept. AGNSS provides the navigation message at a faster data rate than the GNSS satellites do, while adding some extra assistance information for helping and boosting the indoor acquisition process. Note that in the absence of such a help (what is referred to as a cold start), a GNSS receiver may require about 1 min before issuing the first position fix. This value is reduced down to less than 1 s when appropriate knowledge, such as the almanac, ephemerides, and a fine-enough initial guess of the user's position, Doppler, and time, is available (situation that is referred to as a hot start) [48].

SIGNAL PROCESSING TECHNIQUES FOR INDOOR GNSS RECEIVERS

EXTENDED CORRELATION

It is clear that to be eventually able to detect weak signals, there is no choice but to accumulate the signal energy during long observation intervals. This is the so-called HS-GNSS principle, and it is based on improving the receiver sensitivity through the use of extended correlations combining coherent and non-CIs. Assuming henceforth a digital receiver, extended correlations are based on evaluating the following noncoherent accumulation:

$$R_{\mathrm{NC}}(\tau, f) \doteq \frac{1}{N_I} \sum_{k=0}^{N_I-1} |R_C(\tau, f; k)|^2, \tag{9}$$

where the coherent correlation $R_C(\tau, f; k)$ is defined as

$$R_C(\tau, f; k) \doteq \sum_{n=\lfloor kN_C N_{\mathrm{scode}} \rfloor}^{\lfloor (k+1)N_C N_{\mathrm{scode}}-1 \rfloor} [x(n)c(((1+f/f_x)n-\tau)_{\mathrm{mod}N'_{\mathrm{scode}}})e^{-j2\pi fn} \tag{10}$$

with $c(n) \doteq c_c(nT_s)$ the discrete-time version of the local code replica, $\{N_C, N_I\}$ the number of coherent and non-CIs, respectively, and $N'_{\mathrm{scode}} \doteq \mathrm{round}(N_{\mathrm{scode}})$. The total integration or dwell time becomes $T_{\mathrm{tot}} = N_I N_C N_{\mathrm{scode}} T_s$ and the evaluation of the extended correlation in (9) depends on the tentative time-delay and Doppler frequency shift $\{\tau, f\}$. At the acquisition stage of a HS-GNSS receiver, the satellite under analysis is declared to be present (i.e., it is acquired) when $R_{NC}(\tau, f) > \gamma$, for a given threshold γ specified by the user-defined probability of false alarm P_{FA}. This detection process automatically provides coarse estimates for the unknown time-delay and frequency shift errors as

$$(\hat{\tau}_{\epsilon,0}, \hat{f}_{d,0}) = \arg \max_{\tau,f} R_{\mathrm{NC}}(\tau, f) \quad \text{s.t.} \quad \max_{\tau,f} R_{\mathrm{NC}}(\tau, f) > \gamma. \tag{11}$$

It is important to remark that the time-delay estimates $\hat{\tau}_{\epsilon,0}$ correspond to the fractional part of the true time-delay τ_0 within a code period. That is to say, $\tau_{\epsilon,0} \doteq [\tau_0]_{N'_{\mathrm{scode}}}$ with $[\cdot]_N$ the modulus N operation, and $\tau_{\epsilon,0} \in [0, N'_{\mathrm{scode}} - 1)$. The GNSS receiver has to determine the number of elapsed code periods since the signal was transmitted, and add this coarse delay to the result from (11). This problem is solved at the navigation module of the receiver and it will be discussed later on in the section "Synthetic Recovery of the Signal Time Stamps." Notwithstanding, it is not convenient to select right away the maximum of (11) as the correct solution because further processing to combat near-far effects still needs to be done.

Finally, it is also interesting to point out that the extended correlation in (9) can be replaced with the product of two consecutive accumulated values for k and $k+1$, respectively. This approach is called differential correlation and it offers an average sensitivity gain of 1.5 dB when data bits are a priori known [49]. Unfortunately, the assumption of a priori known data bits barely holds true in most practical indoor GNSS receivers, and it is indeed the extended correlation in (9) what is mostly implemented. There are, however, some limitations regarding the evaluation of (9) that must be taken into consideration.

LIMITS ON THE COHERENT INTEGRATION

It was already introduced in the section "Acquisition" that CI is limited to a fraction of the bit interval due to the presence of unknown data bit transitions. A common practice is to adopt the half-bit method, which consists of using two consecutive pieces of signal of $T_d/2$ seconds for implementing two separate CIs [50]. This guarantees that at least one of the two integrations will not be affected by the bit transition, and a CI of $T_d/2$ can be assured. The full-bit method is an alternative approach that exploits the cyclostationary properties of the received signal to synchronize with the bit transition boundaries and thus be able to perform full CIs during the whole bit period [50]. The bit alignment can also be achieved by implementing a traditional bit synchronizer, which boils down to a multiple hypothesis testing problem where each hypothesis is represented by a time shift equal to the primary code duration. The price to be paid is a high computational burden due to the evaluation of all N_r possible hypotheses.

Even in the case of having bit synchronization, the received bits are still unknown to the receiver and some other limitations to extend the CI beyond one bit interval do appear [51, Ch. 4]. There are data-aided (DA) and non-DA (NDA) signal processing techniques to cope with this problem. DA techniques

remove the bit contribution from the received signal by using some prior knowledge on the actual bits being received. This prior knowledge can be provided by AGNSS servers as part of the assistance information, but this approach is not the preferred solution due to many implications at the system level. First, the GNSS receiver needs a continuous access to the AGNSS server whenever it wants to compute a position fix. Second, the transmission from the AGNSS server has to be roughly bit-synchronized with the GNSS navigation message as received from the satellites [52, Ch. 7]. Otherwise, if the AGNSS assistance data is not used for data wipe off, the receiver can keep it and use it later on to compute a position-fix even if at that instant it has no access to the communication subsystem. Actually, a current research topic is the design of assistance information formats with longer validity periods so as to reduce the need for connectivity as much as possible. In the near future, the existence of pilot symbols in Galileo and modernized GPS signals should seemingly allow the implementation of DA techniques for extending the CI. Unfortunately, the receiver will need to synchronize first with the secondary code, which adds an extra and nonnegligible complexity to the whole problem [53]. NDA synchronization techniques solve this limitation by focusing on the exploitation of the statistical properties of the received signal. No explicit knowledge on the data bits is required. Although these so-called blind methods have been widely studied in the context of digital communications, it is not known whether and how they could be applied to GNSS signals indoors. This issue constitutes another open line of research.

NEAR-FAR DETECTION TECHNIQUES ARE AIMED AT DISCRIMINATING BETWEEN THE CORRELATION PEAKS CORRESPONDING TO THE DESIRED SIGNAL AND CROSS-CORRELATION PEAKS CAUSED BY A STRONG INTERFERING SIGNAL.

LIMITS ON THE NONCOHERENT INTEGRATION

In view of the limitations of CI, it might be argued that it should be possible to attain the required sensitivity by increasing the non-CI without bound. This argument, although theoretically valid, is flawed because of some real-world implementation aspects that are generally overlooked in analytical derivations of conventional receivers. Increasing the number of non-CIs has two main impacts. First, it can easily result in TTF values exceeding far beyond the acceptable user limits. Second, it puts some constraints on the required Doppler estimation accuracy, which must be on the order of the total integration time, T_{tot} and not on the reciprocal of the CI time as usually assumed in communication systems. It is true that the amplitude of the correlation peak depends on how accurate the Doppler estimate is, but in a positioning receiver, we are not only interested in detecting the signal (as it happens in most communication systems) but also in determining as exactly possible the time-delay τ_0. An error in the determination of the Doppler shift has an impact in the baseband signal via the term $c(((1+f/f_x)n-\tau_0)_{\text{mod}\,N'_{\text{scode}}})$ and it is equivalent to a mismatch between the chip duration of the received signal and that of the local code replica. When this mismatch is carried over a large integration interval, the result is a small time shift between the consecutive correlation peaks to be noncoherently integrated, which blurs the resulting total correlation and introduces a bias in the final estimate of τ_0. Although the difference between both chip durations is very small in relative terms, the accrued effect may become on the order of the chip duration (i.e., 300 m for GPS-L1 C/A signals) unless the receiver signal processing algorithms are properly dimensioned.

We have experimentally confirmed that it is necessary that $T_{\text{tot}} \leq 2\Delta\tau\ (F_x/\Delta F)$, where $\Delta\tau$ is the maximum tolerable error in time-delay estimation due to errors in the Doppler shift estimation, and $\Delta F = 1/(2T_s N_{\text{scode}})$ is the coarse Doppler search resolution. Nevertheless, even if a finer Doppler search is implemented, T_{tot} cannot be increased without bound because the true Doppler shift $F_{d,0}$ cannot be considered to be constant due to clock drift instabilities. The way to overcome this problem is by using methods to estimate the clock dynamics, but this solution is not feasible in handheld receivers. Current clock technology limits the integration period to less than 10 s, and it is recognized that the development of more accurate and cost-effective clocks will be a key technological enabler of indoor GNSS solutions with increased sensitivity [54]. There are other effects that limit the maximum value of T_{tot}. The satellites, and possibly the receiver, are moving during the correlation time. However, the result of processing the received signal during T_{tot} seconds is only one single time-delay per satellite. The position fix provided by the receiver using these time-delays has an intrinsic uncertainty in the time instant to which it corresponds. It is a kind of average of the positions along the whole correlation time rather than the position at a specific time instant. The same type of ambiguity appears when choosing the time instant at which to compute the satellite positions, either the time at the starting point of the correlation, at the middle, or at the end.

EFFICIENT FFT-BASED IMPLEMENTATION

The correlation between the input signal and the local replica is certainly the most time-consuming operation within the acquisition stage. It involves the product of typically thousands of samples per millisecond for each of the correlation lags, frequency bins, and satellites to be evaluated. The situation becomes even worse indoors, where full CI is sought and bit synchronization is desired. Correlations are usually implemented in the frequency domain to avoid such a high computational burden. That is, multiplying the frequency domain representations of both the incoming signal and the local code, instead of performing the whole process in the time domain by using shifts, multiplications, and add operations. Frequency representations are obtained using the N-sample fast Fourier transform (FFT), an efficient implementation for which complexity

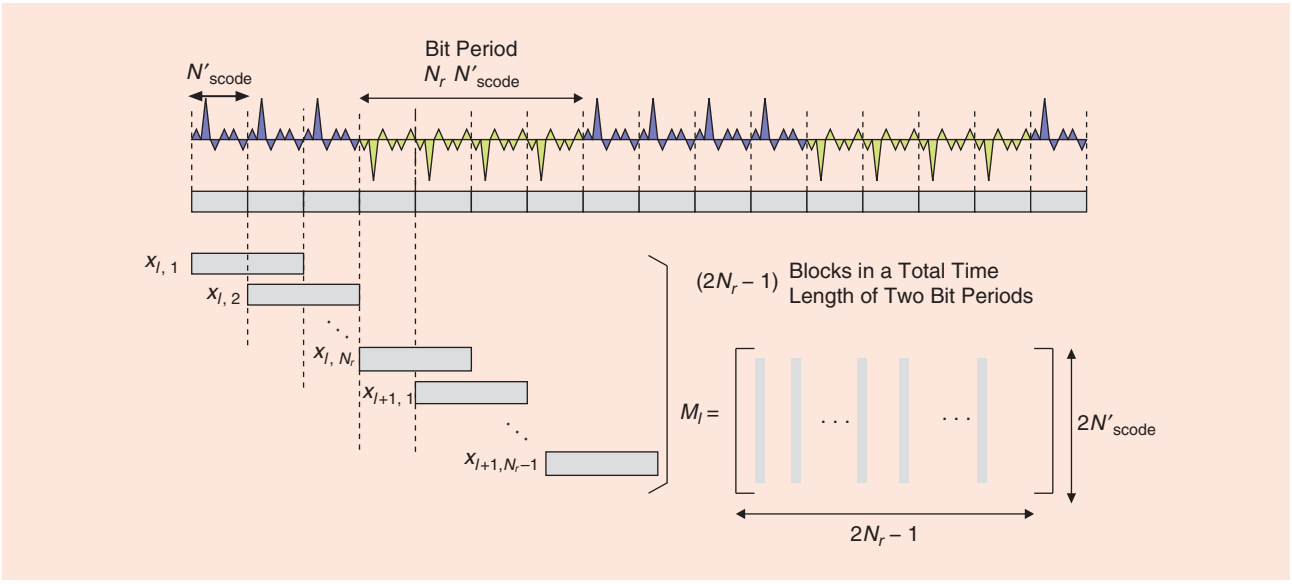

[FIG10] **Procedure to fill the data matrix $\mathbf{M}_l$ used in the double-FFT HS acquisition algorithm in [46].**

reduces down to $O(N \log N)$ operations compared to $O(N^2)$ of the traditional discrete-time Fourier transform (DFT) and time-domain correlation.

Many FFT-based implementations for the acquisition stage of GNSS receivers have been proposed in the literature using a snapshot or block-processing perspective [50], [55]–[57]. In [51], two algorithms for implementing extended correlations are presented, either making extensive use of circular correlations or by using double block zero padding (DBZP) FFT implementations. The latter approach is also proposed in [58], reporting sensitivity values down to $C/N_0 = 15$ dB-Hz. In this case, CI is extended over multiple bits by using a bit combination template that consists of negative and positive ones. CI is performed for each combination of bits, and the most likely sequence is taken as the one resulting in the highest correlation output power. Although a good performance is reported, the main drawback of this method is that it is computationally intensive and errors in determining the correct bit sequence may completely degrade the code-delay and frequency estimates due to a severe energy loss at the correlator output [59].

In [46], an algorithm was proposed that is capable of providing a full bit-interval CI without any prior knowledge about bit transitions. The so-called double-FFT method can be efficiently implemented with only simple operations such as additions, products, circular shifts, and the extensive use of FFT processors. Moreover, it can also be understood as the optimal time-frequency matched filter to the input signal, and the steps to be followed are described next.

FFT-BASED CODE CORRELATION

The first step is to take a block of samples with a duration of two bit periods to assure that a whole bit will be contained within the block. Then, pieces of $2N_{\text{scode}}$ samples taken every code period are column-wise stacked to build a matrix, $\mathbf{M}_l \in \mathbb{C}^{2N_{\text{scode}} \times (2N_r - 1)}$, as shown in Figure 10, with the subscript l corresponding to the bit interval being processed. The matrix $\mathbf{M}_l$ will be used in the FFT-based correlation, which is implemented via the overlap-save method. This method offers an efficient way of performing a blockwise correlation/convolution operation between a continuous stream of samples and a finite length data block [60].

Because of either residual Doppler or a noncommensurate sampling rate, the received signal code period may result in a noninteger number of samples per code, N_{scode}. This effect causes some uncertainty when filling the columns of $\mathbf{M}_l$, since it is not clear at all what the true first sample of each code period is. The easiest solution is to $N'_{\text{scode}} \doteq \text{round}(N_{\text{scode}})$ and start filling each column of $\mathbf{M}_l$ at multiples of this value. However, proceeding in this way introduces a small time-delay error that propagates from column to column. This time delay will cause the correlation peaks not to be aligned with each other, and a penalty loss will occur later on, when all peaks are added together. It is a similar effect to the correlation blurring already mentioned when discussing the limits on the non-CI in the section "Limits on the Noncoherent Integration." To have an idea here on the order of magnitude of the incurred error, it suffices to say that typical sampling rates provide two to four samples per chip, which for the most optimistic case, provides the equivalent of 75 m of distance from sample to sample in GPS-L1 C/A signals. Thus, subsample roundoff errors may bias the current pseudorange measurement in ± 37.5 m. To avoid such a peak misalignment, interpolation techniques must be applied onto each column of $\mathbf{M}_l$ prior to the FFT-based correlation. These techniques can easily be implemented in the frequency domain by the element-wise product of each column of $\mathbf{M}_l$ with an appropriate set of complex exponentials, which represent the phase shifts incorporated in matrix $\mathbf{T}_l$.

When the FFT-based correlation is done, the resulting time-domain correlation samples are stacked into a matrix $\mathbf{Y}_l(f_i) \in \mathbb{C}^{2N'_{\text{scode}} \times (2N_r - 1)}$. The overall process can be mathematically formulated as [61]

$$\mathbf{Y}_l(f_i) \doteq \mathbf{F}^H\left[(\mathbf{F}\mathbf{M}_l) \odot \mathbf{T}_l \odot \left((\mathbf{J}_i \mathbf{F}\mathbf{c}) \otimes \mathbf{1}^T_{2N_r - 1}\right)\right], \tag{12}$$

where $f_i \doteq i\Delta f - \mathrm{F}_{d,\,\max}$ is the tentative Doppler being tested with $i = \{0, 1, \ldots, N_{f\text{bins}} - 1\}$ and $F_{d\max}$ is the maximum Doppler shift. $\mathbf{F}$ is the DFT matrix (i.e., in practice, an FFT operation), $\odot$ the Schur-Hadamard or element-wise product, $\otimes$ the Kronecker product, $\mathbf{c}$ the vector of samples with the GNSS code, $\mathbf{1}_N$ an $(N \times 1)$ all-ones vector, and $\mathbf{J}_i$ applies a circular shift of i samples. Note that circularly shifting i samples into the frequency representation of the GNSS code can be viewed as a frequency shift of $i\Delta f$. Typically for indoor GPS-L1 receivers, $\Delta f = 500$ Hz. Even when assistance information is available, a few coarse Doppler bins are scanned to account for the possible clock drift of the receiver. For handheld receivers with 1 ppm clock stability, it involves $F_{d,\max} = 1.5$ kHz and $N_{f\text{bins}} = 7$.

FULL-BIT COHERENT INTEGRATION

Once $\mathbf{Y}_l(f_i)$ is available, the next step is to search for the bit transition to perform a full-bit CI. The process is illustrated in Figure 11, where a sliding window of one bit duration is used to coherently integrate the correlation outputs by moving in steps of N_{scode} samples. The step indexation for the bit transition search is indicated as $m = \{0, 1, \ldots, N_r - 1\}$. Note that due to the overlap-save correlation method, just the upper half of $\mathbf{Y}_l(f_i)$ does really correspond to the circular correlation and the lower half can be discarded. Moreover, the CI to be carried out by the sliding window needs to be done for different fine frequency shifts, which calls for the use of a row-wise FFT within the window, as indicated in Figure 11. The size of this second FFT is the column size of the sliding matrix, N_r, but usually N_r additional zeros are appended to each row and a zero-padded $2N_r$-FFT is carried out instead. This provides a finer frequency resolution of $\Delta f_{\text{fine}} = 1/(2N_r N'_{\text{scode}} T_s)$. For the case of GPS-L1 C/A signals $(N_r = 20)$, the fine frequency resolution of this acquisition method becomes 25 Hz.

The result of the second FFT is a matrix $\mathbf{R}_l(i, m) \in \mathbb{C}^{N_{\text{scode}} \times 2N_r}$ with i the coarse Doppler bin, l the bit period, and m the bit transition position under analysis. Since this process must be repeated for all the coarse time-frequency hypotheses $\{i, m\}$, and during many bit intervals in a noncoherent manner (to be described in the next step) the output samples need to be conveniently stored in a 3-D matrix $\mathcal{R}_l(i)$ with dimensions $(N'_{\text{scode}} \times 2N_r \times N_r)$. This matrix is also referred to as the acquisition hypercube in [46], and it contains the required data for issuing a final decision regarding the acquisition of the satellite under analysis.

NONCOHERENT INTEGRATION

The final step in the FFT-based acquisition method of [46] involves increasing the overall integration interval by means of noncoherent accumulations. This is done by accumulating the squared values of the acquisition hypercube matrices for consecutive bit periods

$$\mathcal{R}_{\text{NC}}(i) \doteq \frac{1}{N_I} \sum_{l=0}^{N_I - 1} |\mathcal{R}_l(i)|^2. \tag{13}$$

Finally, the maximization in (11) can be reformulated as a grid-search process

$$(\hat{m}_0, \hat{\tau}_{\epsilon,0}, \hat{i}_0, \hat{f}_{\epsilon,0}) = \arg \max_{m, \tau_\epsilon, i, f_\epsilon} [\mathcal{R}_{\text{NC}}(i)]_{\tau_\epsilon, f_\epsilon, m}$$
$$\text{s. t} \max_{m, \tau_\epsilon, i, f_\epsilon} [\mathcal{R}_{\text{NC}}(i)]_{\tau_\epsilon, f_\epsilon} > \gamma, \tag{14}$$

where $m = \{0, \ldots, N_r - 1\}$ searches for the bit transition alignment, $\tau_\epsilon = \{0, \ldots, N'_{\text{scode}} - 1\}$ for the residual time-delay within one code period, $i = \{0, \ldots, N_{f\text{bins}} - 1\}$ for the coarse Doppler bin, and $f_\epsilon = \{0, \ldots, 2N_r - 1\}$ for the fine frequency bin. The coordinates of the maximum peak in (14) provide the Doppler shift and time-delay estimates for the received signal. In particular, $\hat{F}_{d,0} = \hat{i}_0 \cdot \Delta f - F_{d,\max} + \hat{f}_{\epsilon,0} \cdot \Delta f_{\text{fine}}$ (Hz) whereas $\hat{\tau}_0 = \hat{m}_0 N'_{\text{scode}} + \hat{\tau}_{\epsilon,0} + \tau_{\text{ambig}}$ (samples), with some remaining ambiguity τ_{ambig} that must be solved by using the time stamps on

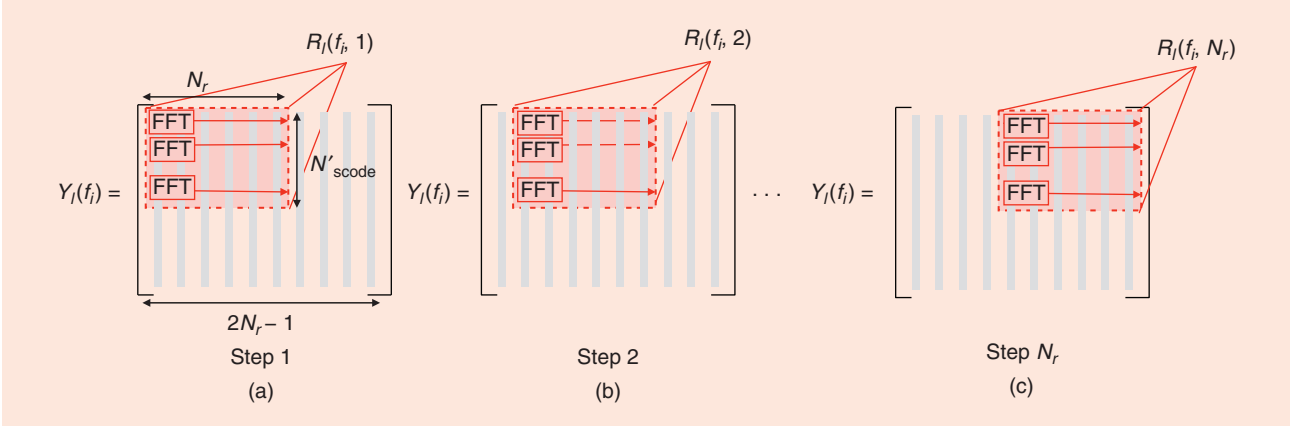

[FIG11] Parts (a)–(c) show the procedure for coarse bit synchronization in the double-FFT HS acquisition algorithm.

the navigation message or the method described later on in the section "Synthetic Recovery of the Signal Time Stamps."

FINE ACQUISITION

The determination of the correct peak in (14) has to be done as accurately as possible and, for the sake of simplicity, it is often reasonable to perform first a coarse search followed by a more accurate one. Unlike conventional receivers, where acquisition is followed by tracking, in HS-GNSS receivers no tracking is usually implemented but rather a snapshot-based (i.e., acquisition only) architecture. The lack of tracking does not imply that the acquisition process finishes when (14) is solved, but on the contrary, further refinements are still to be carried out in the so-called fine-acquisition stage.

The goal of fine acquisition is to improve the accuracy of the grid search estimates provided by (14), which is intrinsically limited by the FFT-based acquisition architecture. For instance, the resolution of the fine Doppler estimate depends on the reciprocal of the second FFT length, and the resolution of the residual time-delay estimate is limited by the sampling period. The latter estimate, the residual code-delay, can indeed be refined while keeping the sampling rate constant. The next two different approaches can be followed.

RESAMPLING

It consists of recalculating some correlation points around the code delay estimate provided by (14) using the formal definition of the extended correlation introduced in (9). This recalculation (using the linear correlation instead of the circular one) is done at the end of the acquisition process because it is then when we have available an estimate of the Doppler shift $\hat{f}_{d,0}$. Some few new correlation points can be recalculated more precisely because the local replica can incorporate the Doppler shift estimate both in the carrier and in the PN code.

ALGEBRAIC CORRECTION

It is an alternative approach that considers the Doppler effect on the code as a time-delay. Thus, once the Doppler shift is known at the end of the acquisition stage (both in its coarse and fine contribution), the code-delay estimate $\hat{\tau}_0$ can be refined by applying a correction term that takes into consideration the delay produced by the presence of a residual frequency error during the whole extended correlation interval in (9). The corrected time-delay results in

$$\hat{\tau}_{0,ac} = \hat{\tau}_0 + \frac{\hat{f}_{d,0}}{f_x}\frac{N_I N_C N_{\text{scode}}}{2}. \tag{15}$$

After either resampling or algebraic correction, the available correlation values around the new maximum peak can be interpolated for determining the position where the true correlation peak is located. It is the amplitude of these more accurate points that is crucial rather than their time-domain positions, since any amplitude error will eventually appear as an error in the position of the maximum peak after interpolation. This is why a finer grid in the time domain is not needed. Any interpolation method, such as polynomial or bandlimited techniques, may be used. We advocate using a piecewise linear interpolator that fits a triangle to three refined correlation points and computes the position of the vertex. That is,

$$\hat{\tau}_{0,\,\text{interp}} = \hat{\tau}_0 + \frac{1}{2}\frac{R_{\text{NC}}(\hat{\tau}_0+1,\hat{f}_{d,0}) - R_{\text{NC}}(\hat{\tau}_0-1,\hat{f}_{d,0})}{R_{\text{NC}}(\hat{\tau}_0,\hat{f}_{d,0}) - \min\{R_{\text{NC}}(\hat{\tau}_0+1,\hat{f}_{d,0}), R_{\text{NC}}(\hat{\tau}_0-1,\hat{f}_{d,0})\}}. \tag{16}$$

It has been shown that this simple interpolator yields an accuracy comparable to that of more sophisticated methods at a reduced complexity, and it approaches the Cramér-Rao bound [28].

NEAR-FAR DETECTION AND MITIGATION

Near-far detection techniques are aimed at discriminating between the correlation peaks corresponding to the desired signal and cross-correlation peaks caused by a strong interfering signal. As such, the most appropriate step at which near-far detection must be implemented is the acquisition stage, where the acquisition hypercube is still available and plenty of correlation samples can be used for statistical analyses. Indeed, one of the common approaches for near-far detection is based on the different statistics of the squared cross-correlation samples $R_{\text{NC}}(\tau, f)$, in the presence and in the absence of near-far. When near-far is absent, the statistics of $R_{\text{NC}}(\tau,f)$ for $|\tau - \tau_0| > T_c$ are dominated by thermal noise. They follow a χ^2 distribution, and the probability that $R_{\text{NC}}(\tau,f)$ surpasses a given threshold γ_{nf} can be calculated exactly. When near-far is present, the statistics of $R_{\text{NC}}(\tau,f)$ are dominated by the cross-correlation between the interfering signal and the code replica, resulting in a statistical distribution with heavier tails that differs much from the previous one. Many correlation peaks will now surpass the previous threshold γ_{nf}, thus violating the surpassing probability and making explicit the presence of near-far [28].

For low-complexity handheld receivers, there are simpler ways to take advantage of the statistical differences in the absence and presence of near-far. For instance, near-far may be declared when the distance between the two largest correlation peaks in the acquisition hypercube is less than a given threshold [62]. Preliminary results show that this method is simpler and performs slightly better than relying on the probabilities of threshold surpassing. Another approach in [63] exploits the frequency and time variation of near-far due the time variation of relative delays and frequency shifts across satellites. This suggests that near-far detection has to be repeated for each coarse and fine Doppler shift, and for each bit alignment hypothesis in (14). In any case, the design of near-far detectors and the characterization of their probability of detection and false alarm constitutes an open problem. The statistical characterization of near-far is very difficult, and it remains to be

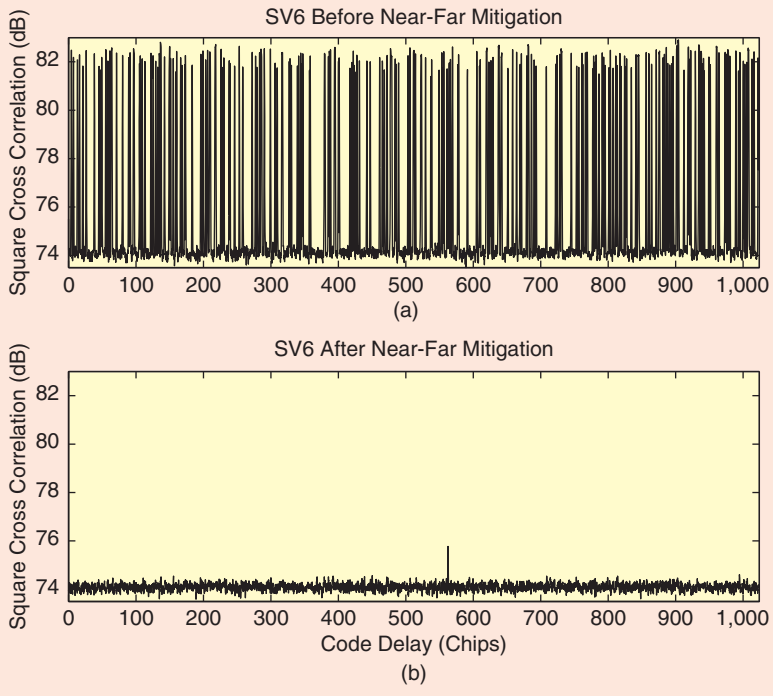

[FIG12] Example of near-far corrupted correlation samples as a function of τ (in chips), before and after applying the near-far mitigation technique in [28]. The weak signal corresponds to the GPS-L1 SV6 with $C/N_0 = 20$ dB-Hz and there are two strong signals, GPS-L1 SV3 with $C/N_0 = 55$ dB-Hz and GPS-L1 SV17 with $C/N_0 = 50$ dB-Hz.

known the goodness of the proposed approximations in real-life working conditions.

Once near-far detection has been applied to the acquisition hypercube, the typical situation is that only one or none of the candidate peaks will be declared free of near-far. Nevertheless, if more than one peak is considered not to be caused by near-far, the one with the largest amplitude with respect to the first threshold should be selected. If near-far is detected in all the candidate peaks, the signal may be cleaned using near-far mitigation techniques as shown in Figure 12. Existing proposals inherit the existing background in multiuser detection techniques for CDMA wireless communications. The common approaches are based on the idea of successive interference cancellation (SIC), where the strongest satellite signals are first detected and then removed one after another from the overall received signal [64], [28]. Parallel implementations (PICs) [65] and subspace projection methods [66] have also been proposed, but the required complexity is much higher and their practical application is compromised by the limited computational power of most commercial receivers. It is for this reason that before using any of these computationally demanding algorithms, it seems reasonable to try first to identify those satellites whose acquisition is envisaged to be interfered by other more powerful ones. This can be done by measuring the received signal strength (see the section "Signal Strength Measurement"). After this identification process one can decide either to discard the affected satellites, which is often enough, or to rescue them by applying near-far mitigation techniques. For the latter, research onto low-complexity near-far mitigation techniques is still an open research line.

The near-far problem has been reduced with Galileo and modernized GPS signals due to the adoption of longer spreading codes that provide between 6–30 dB of increased cross-correlation protection. The range is so wide because it depends on the signal component to be considered and on whether coherent correlation extends to the complete secondary code or only to the primary one. Notice however that this gain is obtained at the price of a more complex coarse acquisition (i.e., two codes must be acquired, the primary and the secondary). Altogether it is not clear if one gain will be offset by this and other disadvantages, and hence to which extent Galileo and modernized GPS will make possible the development of better and simpler indoor receivers.

SIGNAL STRENGTH MEASUREMENT

Measuring the received signal strength is an essential part of any GNSS receiver. It is required, for instance, when computing the user's position based on the set of available time-delay estimates. In this case, a weighted least squares (WLS) approach is adopted, where the time-delay estimate from each satellite is weighted by the square root of the corresponding signal strength. Signal strength monitoring is also required as a form of lock detection in GNSS tracking loops, to ascertain whether the GNSS signal is being tracked or not. For HS-GNSS, near-far mitigation techniques often make use of signal strength estimates, which are used to distinguish between weak and strong satellites, and thus are able to detect potentially harmful interference sources to the acquisition of weak signals.

Being related to the SNR, signal strength estimates in terms of C/N_0 suffer from the same limitations of SNR estimates. That is, they are generally biased and exhibit a large variance due to their implementation as ratios of quadratic forms. The way to overcome this limitation in practice is to increase the processed signal length until bias and variance are much smaller than the actual values of SNR or C/N_0 to be measured. However, as it occurs at the acquisition stage, this approach may be not feasible at all because the required signal length may be too large. An important limitation of C/N_0 estimators is their poor performance when implemented in indoor GNSS receivers, where biases on the order of 20 dB are commonly found. The reason for such a degradation lies in the very fundamental structure of most C/N_0 estimators. They are based on a coherent post-correlation approach where C/N_0 is estimated at the correlation output,

where both code-delay and Doppler shift are optimistically assumed to have been accurately compensated [67]. This is the case, for instance, of the well-known narrowband-wideband power ratio (NWPR) method in [8, Ch. 8], with the C/N_0 being estimated as

$$\left(\frac{\hat{C}}{N_0}\right)_{\text{NWPR}} \doteq \frac{1}{T_s}\frac{\hat{\mu}_{\text{NP}}-1}{N_c-\hat{\mu}_{\text{NP}}}, \tag{17}$$

where $\hat{\mu}_{\text{NP}} \doteq (1/K)\sum_{k=1}^{K}\text{NP}_k$ is the mean of power ratios defined as $\text{NP}_k \doteq \text{NBP}_k/\text{WBP}_k$, with $\text{NBP}_k \doteq |\sum_{i=0}^{N_c-1} R_C(\hat{\tau}_0, \hat{f}_{d,0}; i)|^2$ and $\text{WBP}_k \doteq \sum_{i=0}^{N_c-1}|\text{R}_C(\hat{\tau}_0, \hat{f}_{d,0}; i)|^2$ the so-called narrowband and wideband powers, respectively. Apart from the residual errors in the delay and Doppler estimates, which degrade inevitably the accuracy of the NBP and WBP metrics, the main problem with (17) is that NBP and WBP are too noisy estimates of the corresponding powers due to a lack of sufficient averaging. Note that these parameters take only into account N_c coherent correlations, and the averaging cannot be extended further because of the limitations presented in the sections "Acquisition" and "Extended Correlation." At this point we already know that in indoor usage noncoherent correlations are needed to obtain an acceptable level of signal growth above the noise. So, the question is to devise a C/N_0 estimator that makes use of the non-CIs. The following noncoherent postcorrelation estimator has been proposed in [68]:

$$\left(\frac{\hat{C}}{N_0}\right)_{\text{NC}} \doteq \frac{R_{\text{NC}}(\hat{\tau}_0, \hat{f}_{d,0})B_n - N_C N_{\text{scode}}\hat{P}/T_s}{(N_C N_{\text{scode}})^2\hat{P} - R_{\text{NC}}(\hat{\tau}_0, \hat{f}_{d,0})} \tag{18}$$

with B_n the receiver noise bandwidth and $\hat{P}$ an estimate of the input signal power. This estimator employs only quantities that are readily available in an indoor receiver and thus it does not require any additional complexity. The bias is found to be smaller than 1 dB-Hz for all possible values of C/N_0 down to the receiver sensitivity (normally between 10 and 20 dB-Hz), and the variances become very close to the CRB for large C/N_0 values [28].

Some other estimators have been proposed in the literature where the relationship between some intermediate values computed in the receiver and C/N_0 are exploited. The interested reader may find a valuable summary of these and other techniques in [69].

SYNTHETIC RECOVERY OF THE SIGNAL TIME STAMPS

As already discussed in the section "Signal Attenuation," one of the consequences of operating GNSS receivers indoors is the impossibility to decode the navigation message and thus, to retrieve the signal time stamps. Without this information, indoor GNSS receivers are not able to refer their time-delay estimates to the absolute GNSS time scale, causing the resulting pseudoranges to be ambiguous. Actually, the ambiguity represents the shift between the signal features that the receiver is able to observe at low SNR (e.g., the start of the PN code or the bit edges) and those that cannot observe (i.e., the time stamps conveyed by the navigation message). The value of the ambiguity is a multiple of a given basic distance, which is determined by the specific signal structure, since it is this structure that defines the possible separations between the observable and nonobservable features. For the case of GPS-L1 C/A, the ambiguity is a multiple of approximately 6,000 km (the distance equivalent to one bit period of 20 ms duration) or 300 km (the distance equivalent to one code period of 1 ms duration) depending on whether the bit synchronization has been implemented and achieved or not, respectively.

MEASURING THE RECEIVED SIGNAL STRENGTH IS AN ESSENTIAL PART OF ANY GNSS RECEIVER.

In terms of the mathematical formulation presented in the section "Foundations of GNSS Positioning," the measured pseudoranges in (1) can be expressed as

$$d_i = \rho_i + k_i D_{\text{amb}} + c\delta t_u + c\delta t_{n,i}, \tag{19}$$

where k_i is an a priori unknown positive integer, D_{amb} is the basic ambiguous distance (e.g. the 300 or 6,000 km previously mentioned). Due to the ambiguity, d_i are called fractional pseudoranges.

A possible way to obtain the value of k_i is based on the fact that the disturbances $c\delta t_{\epsilon,i}$ are usually much smaller than D_{amb}. Assuming also that an approximate value $\rho_{i,0}$ of the range is available, the values of k_i can be readily computed by rounding the difference $(d_i - \rho_{i,0})/D_{\text{amb}}$. Note that having such an approximate a priori value of ρ_i is not a problem because the uncertainties in the satellite position $\mathbf{r}_{s,i}$ and the receiver position $\mathbf{r}_u$ are much smaller than D_{amb} thanks to the assistance information. This way of fixing the values k_i implies that δt_u represents the fractional part of the clock offset, and it is necessarily confined within $[-0.5\,D_{\text{amb}}/c,\ 0.5D_{\text{amb}}/\text{c})$, otherwise the factors k_i would not be unique.

It may seem that once the values of k_i are determined, the position determination falls back to the conventional case described in the section "Foundations of GNSS Positioning." However, there is a key subtlety that completely changes the navigation solution. The satellite position used in the computation of ρ_i shall be the satellite position at the transmit time of the signal, that is, $\mathbf{r}_{s,i}(t_{s,i})$. The transmit times $t_{s,i}$ are not known because the time stamps are not available at the receiver. The navigation solution with unknown transmit times is a topic that would deserve a full paper by itself. To the authors' knowledge the best treatment of this issue can be found in [52, Ch. 4]. We are going to describe here two techniques representative of two families of solutions available. In all cases, the underlying basic principle is the fact that even in the case of measuring fractional pseudoranges, in the absence of measurement disturbances there is a unique position and time combination for which the fractional pseudoranges could have been observed.

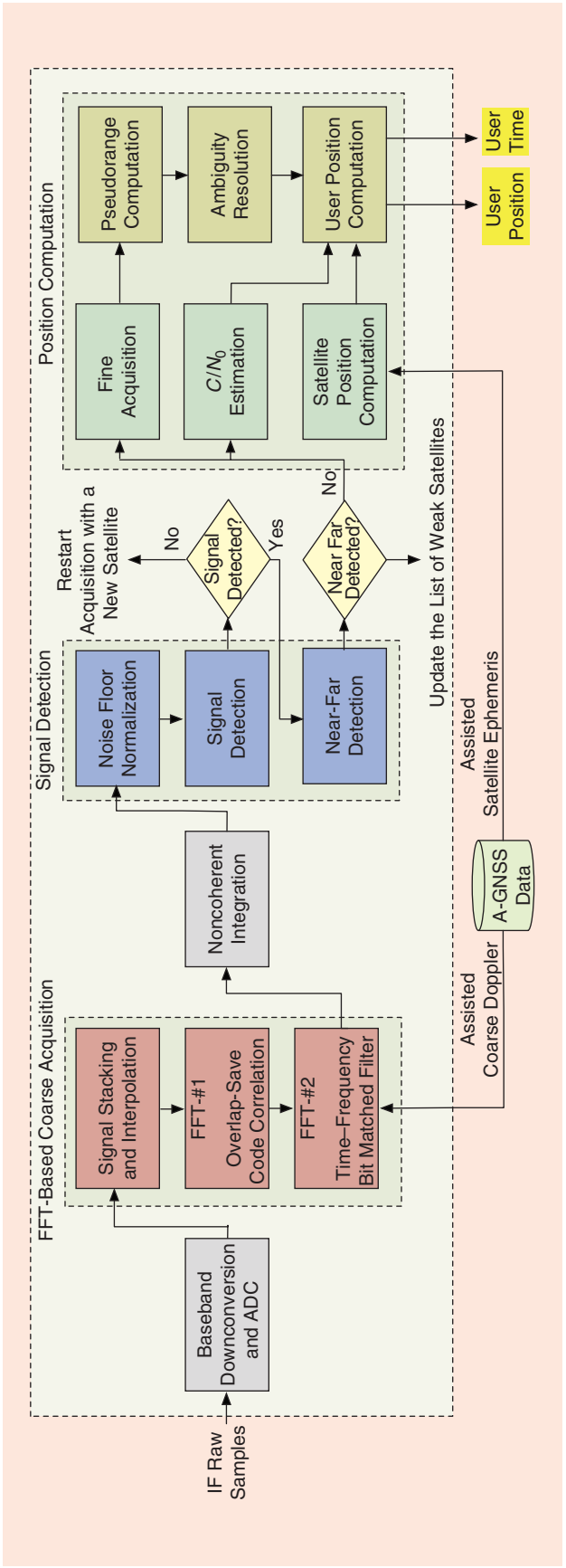

[FIG13] Architecture of an indoor GNSS snapshot receiver illustrating the sequence of signal processing techniques to be carried out to obtain the user's position.

The algorithm in [70] is an exact but brute-force solution of a least-squares problem with an integer unknown. It is simply based on an enumeration procedure, where the least-squares problem is solved for all possible values of the integer variable, and the one providing the smallest residual is selected. In our case the integer variable is given by the ambiguity in the transmit times $t_{s,i}$ of the satellites, where the ambiguity is a multiple of D_{amb}/c, but it is not k_i. Note that the ambiguity in the transmit times is the same for all satellites, unlike what happens with k_i, that is the ambiguity is each pseudorange and is satellite dependent. Actually, the computation of k_i is a very easy step, since it involves only a rounding operation, that precedes the actual solution of the navigation equations, so it comes before the brute-force algorithm that we are explaining here and also the computationally simpler described below. It can also be seen that the ambiguity in the transmit times is caused by the fact that any shift multiple of D_{amb}/c applied to both the transmit time and the receiver offset affects the right-hand term of (19) only through ρ_i but not through δt_u, since the shift of the latter can be absorbed by k_i. The algorithm involves therefore a one-dimensional search, where time uncertainty range is divided in multiples of D_{amb}/c. For each multiple, the transmit times of each satellite are shifted by this amount, and they are used to compute the satellites positions. Note that the unshifted value of each transmit time is obtained from the time associated to the observed signal features, which is corrected by $k_i D_{\text{amb}}/c$. For each set of satellite positions, a system formed by several equations like (19) is solved, using for instance the linearization algorithm presented in the section "Foundations of GNSS Positioning" and the time shift candidate showing the best match between the model and the measurements is retained.

A computationally simpler algorithm had been earlier proposed in [71], which is probably the first work addressing the issue of GNSS positioning without time stamps. Unlike the previous technique, in this case there is no need to explore several hypotheses. The basis is to linearize the dependence of ρ_i with the transmit time as follows:

$$\rho_i(\mathbf{r}_{s,i}(t_{s,i}), \mathbf{r}_u) \approx \rho_i(\mathbf{r}_{s,i}(t^0_{s,i}), \mathbf{r}_u) + \frac{\partial \rho_i}{\partial \mathrm{t}_{s,i}} \Delta t_s, \tag{20}$$

where $t^0_{s,i}$ is the unshifted value of the transmit time, the derivative of the distance with respect to the transmit time $\partial\rho_i/\partial\rho_{s,i}$ is by definition the radial velocity of the satellite v_i, and $\Delta t_s = t_{s,i} - t^0_{s,i}$. The key aspect is that Δt_s does not depend on the satellite index i as explained above. After replacing ρ_i in (19) with (20), and linearizing ρ_i also with respect to the tentative user's position $\mathbf{r}_{u,0}$, as done in the conventional method described in the section "Foundations of GNSS Positioning," we obtain

$$\begin{aligned} d_i - \rho_i(\mathbf{r}_{s,i}(t^0_{s,i}), \mathbf{r}_{u,0}) - k_i \mathrm{D}_{\text{amb}} \\ = -\frac{(\mathbf{r}_{s,i}(t^0_{s,i}) - \mathbf{r}_{u,0})^T}{\|\mathbf{r}_{s,i}(t^0_{s,i}) - \mathbf{r}_{u,0}\|} \Delta \mathbf{r}_u + v_i \Delta t_s + c\delta t_u, \end{aligned} \tag{21}$$

where the measured or computed values are on the left-hand side and the unknowns are gathered in the right-hand side, neglecting the noise term $\delta t_{\epsilon,i}$. Therefore, the set of navigation equations can still be formulated as $\mathbf{y} = \mathbf{H}\Delta\mathbf{u}$, with an appropriate redefinition of the terms. Basically, the new observation matrix $\mathbf{H}$ contains an extra column with the velocity of each visible satellite, and the new vector of unknowns $\Delta\mathbf{u}$ contains a fifth unknown representing the uncertainty in the transmission time, Δt_s. This method provides the advantage of a reduced complexity without any performance degradation compared to the first algorithm [72], but this is counterweighted by the fact that at least five satellites in view are required to solve the user's position. It is also interesting to note that the set of velocities v_i can readily be obtained by either calculating variation of the satellite position between two consecutive time instants or using the receiver estimates of the Doppler frequency shift. The latter option is often preferred thanks to a higher stability and simplicity. In either case, there are however some initialization conditions required for the algorithm to converge (note that the process is iterated by taking the computed user position as the new $\mathbf{r}_{u,0}$). Although there is a tradeoff between the required position and time initial accuracy, one can say that approximately the first tentative value of the user's position must be within 100 km of the true position, and the error in the user clock with respect to the GNSS time, and hence also in the transmission time, must be smaller than two minutes. With such a maximum error in the user's position, the determination of k_i is not troublesome at all since the accuracy requirement to be able to compute those values are much looser (i.e., 300 km or more).

INDOOR GNSS RECEIVER ARCHITECTURE

All the signal processing techniques presented so far must be applied according to a state machine that takes into account the variety of situations found in a real scenario. The architecture and flow diagram of a possible receiver implementation is depicted in Figure 13, which has been tested in the framework of the ESA funded project "Signal Processing Techniques and Demonstrator for Indoor GNSS" (DINGPOS) [61]. Results showed that it is possible to acquire GNSS signals down to C/N_0 values of 15 dB-Hz and achieve at the same time a positioning accuracy of a few tens of meters. Research on GNSS does not conclude with the improvement of processing algorithms for GNSS signals in general, which has been the focus of this article. There are many other topics for further research, such as optimal ways of combining multifrequency/multiconstellation measurements, improved processing algorithms at observable level, and the use of carrier-phase measurements for enhanced accuracy in harsh environments, which include also challenges in the broad field of signal processing. From the receiver architecture point of view, it is interesting to point out that concerns on receiver complexity exacerbate when combining multifrequency/multiconstellation measurements, which provide two additional degrees of diversity and thus increase the total number of signals to work with [73]. With more signals to be processed, and longer integration periods for achieving high-sensitivity, the implementation of efficient indoor signal processing techniques arises as another challenge to be faced. In this regard, the extensive use of FFT processors is envisaged as the most cost effective solution to this problem. In line with this topic, the section "Efficient FFT-Based Implementation" has presented an efficient HS-GNSS receiver architecture that performs all the necessary tasks employing only FFT blocks and basic operations. This approach is also aligned with the progressive adoption of graphics processor units for GNSS signal processing, offering a formidable computational power specifically tailored to carry out massive FFT operations [74].

In any case, the search for more accurate and reliable indoor positioning is not brought to an end by the improvement in GNSS only, but there are many other technologies that are suitable and complementary to GNSS, such as WLAN, inertial sensors, and ultrawideband signals. The integration of these technologies and the definition of a complete solution for seamless, cost-effective, and robust indoor positioning still remains an open problem and an active field of research today.

CONCLUSIONS

In this article, we have presented the foundations of existing and planned GNSS systems, putting special emphasis on their signals and receivers. We have provided an overview of the processes that have to be performed to eventually obtain a position fix starting from the electromagnetic waves transmitted by satellites. The analysis of these processes shows that signal processing tasks abound. Sophisticated signal processing algorithms are even more necessary when one intends to extend the use of GNSS beyond the limits of their original designs. This is the case of indoor positioning, where the receiver faces extreme signal attenuation, the presence of multipath, and near-far effects. Combating these indoor-related effects is the starting point for the existing challenges in indoor GNSS signal processing. Multipath detection and mitigation arises as one of the most difficult problems to be tackled. Unlike outdoors, where available methods attempt to cancel out the multipath contribution beyond the LOS component, no LOS component may even be present indoors, and multipath cancellation should be combined with multipath energy extraction to increase the available C/N_0. In that sense, further research is also required for allowing unbiased C/N_0 estimation indoors. This will help the receiver discriminate the strongest satellites' signals and improve the navigation solution by using accurate C/N_0 measurements. Another open problem is the exploitation of sinergies between different stages of the receiver, allowing, for instance, the exchange of soft information between the acquisition and navigation modules. Regarding the exchange of data, and as already discussed in the section "Indoor GNSS Receiver Architecture," indoor GNSS receivers are expected to operate in cooperation with other systems, as a way to circumvent and to cope with many of the adverse indoor propagation impairments being experienced by GNSS signals indoors. Thus, challenges also appear on the

hybridization of multisensor measurements for the provision of seamless and ubiquitous positioning.

Finally, it is important to remark that the use of GNSS in indoor environments, which is the main focus of this article, has generated an intense research effort since there is an indisputable user and commercial demand for it. Most of this effort has been undertaken by the communities traditionally working on GNSS. In this article, we have tried to cast some of the outstanding challenges in the form of detection, estimation, and digital receiver implementation problems to present them in a way that is familiar to the signal processing community and to attract its attention. We believe that there are still many questions where our community can provide innovative solutions. We hope that this feature article will serve to unveil the core features of indoor GNSS signal processing, allow the reader to proceed with the development of new algorithms, and, eventually, to spark new research on the topic.

ACKNOWLEDGMENTS

This work was supported by the European Space Agency (ESA) under the DINGPOS contract AO/1-5328/06/NL/GLC and by the Spanish Government under project TEC2011-28219.

AUTHORS

Gonzalo Seco-Granados (gonzalo.seco@uab.es) received the M.Sc. and Ph.D. degrees in telecommunication engineering in 1996 and 2000, respectively, from Universitat Politècnica de Catalunya (UPC). He also received an M.B.A. degree from IESE-University of Navarra, Barcelona, in 2002. From 2002 to 2005, he was a member of technical staff at the European Space Research and Technology Center (ESTEC), ESA, Noordwijk, The Netherlands, involved in the Galileo project and leading the activities concerning indoor GNSS. He has been an associate professor in the Department of Telecomunications and Systems Engineering, Universitat Autònoma de Barcelona (UAB) and member of the Signal Processing for Communications and Navigation (SPCOMNAV) group. He was a guest coeditor for a special issue of *IEEE Signal Processing Magazine* [5]. Since 2009, he has been the director of the chair of knowledge and technology transfer "UAB Research Park—Santander." He is a Senior Member of the IEEE.

José A. López-Salcedo (jose.salcedo@uab.es) received the M.Sc. and Ph.D. degrees in telecommunication engineering in 2001 and 2007, respectively, from UPC. From 2002 to 2006, he was a research assistant at UPC involved in R&D projects related to synchronization techniques for digital receivers, satellite communications, and iterative decoding techniques for MIMO wireless systems, both for private industry and public administrations. Since 2006, he has been an assistant professor in the Department of Telecomunications and Systems Engineering, UAB and a member of the SPCOMNAV group. He is a Member of the IEEE. Since May 2011, he has been coordinator of the telecommunications engineering degree at UAB.

David Jiménez-Baños (david.jimenez.banos@esa.int) received the M.Sc. degree in telecommunication engineering and the M.Sc. degree in information and communication technologies in 2006 from UPC. Since 2006 he has been working at the Radio Navigation Systems and Techniques section of ESTEC, The Netherlands. He is involved in the design and test of GNSS receivers. His main areas of work have been on GNSS signal processing for indoor applications, SBAS systems, and GNSS simulation tools for receiver performance evaluation. He is involved in studying GNSS signal processing techniques for AOCS applications in GEO and higher orbits and GNSS interference modeling and mitigation techniques.

Gustavo López-Risueño (gustavo.lopez.risueno@esa.int) received the M.Sc. and Ph.D. degrees in telecommunication engineering in 1998 and 2003, respectively, from Universidad Politécnica de Madrid (UPM). From 2000 to 2003, he was an assistant professor at UPM working on statistical signal processing for active and passive radars. In 2000 and 2002, he was a visiting researcher at the Adaptive Systems Lab., McMaster University, Canada. From 2004 to 2005, he was a postdoctoral trainee at ESTEC-ESA working on advanced GNSS receivers. In 2006, he joined the NATO Communications, Command, Control Agency, The Netherlands, to work on sensor fusion. Since 2007, he has been a radionavigation systems engineer at ESTEC, The Netherlands, working mainly on signal processing for GNSS receivers, sensor fusion for positioning, and GNSS performance verification and quality monitoring.

REFERENCES

[1] J. Karl, *Celestial Navigation in the GPS Age*. Arcata, CA*:* Paradise Cay Publications, 2007.

[2] R. Schneiderman, "DSPs are helping to make it hard to get lost," *IEEE Signal Processing Mag*., vol. 26, no. 6, pp. 9–13, Nov. 2009.

[3] B. Forsell, *Radionavigation Systems*. Norwood, MA: Artech House, 2008.

[4] M. Sahmoudi, D. Grejner-Brzezinska, F. Gustafsson, G. Lachapelle, R. Landry, and J.-Y. Tourneret, "Guest editorial: Introduction to the issue on advanced signal processing for GNSS and robust navigation," *IEEE J. Select. Topics Signal Processing*, vol. 3, no. 4, pp. 537–540, Aug. 2009.

[5] A. Dogandzic, J. Riba, G. Seco-Granados, and A. L. Swindlehurst, "Positioning and navigation with applications to communications," *IEEE Signal Processing Mag*., vol. 22, no. 4, pp. 10–11, 2005.

[6] H. Wymeersch, J. Lien, and M. Z. Win, "Cooperative localization in wireless networks," *Proc. IEEE*, vol. 97, no. 2, pp. 427–450, Feb. 2009.

[7] P. Biswas, L. Tzu-Chen, T. Kim-Chuan, Y. Ye, and W. Ta-Chung, "Semidefinite programming approaches for sensor network localization with noisy distance measurements," *IEEE Trans. Automat. Sci. Eng*., vol. 3, no. 4, pp. 360–371, Oct. 2006.

[8] B. W. Parkinson and J. J. Spilker, Eds., *Global Positioning System: Theory and Applications*, vol. 1. WA, DC: American Institute of Aeronautics and Astronautics, 1996.

[9] B. Kennes, U. Celestino, and A. Pietka. (2007). *The GNSS market is now! GSA Newslett*. [Online]. 50. Available: http://www.gsa.europa.eu/go/news/the-gnss-market-is-now

[10] F. Viquez and A. Varghese. (2006, Nov./Dec.). *GPS in the GSM handset. When will it become a mainstream? Inside GNSS* [Online]. 36–38. Available: http://www.insidegnss.com/node/862

[11] H. Liu, H. Darabi, P. Banerjee, and J. Liu, "Survey of wireless indoor positioning techniques and systems," *IEEE Trans. Syst., Man, Cybern. C*, vol. 37, no. 6, pp. 1067–1080, Nov. 2007.

[12] *3rd Generation Partnership Project (3GPP)*, "Overview of 3GPP Release 7," v0.9.7, Sept. 2009.

[13] M. Monnerat. (2008, July–Aug.). AGNSS standarization. Inside GNSS [Online]. 22–33. Available: http://www.insidegnss.com/auto/julyaug08-monnerat.pdf

[14] P. Misra and P. Enge, *Global Positioning System: Signals, Measurements and Performance*, 2nd ed. Lincoln, MA: Ganga-Jamuna Press, 2006.

[15] S. Bendrich, P. Defraigne, J. Furthner, J. Hammesfahr, A. Schroth, A. Konovaltsev, A. Bauch, and A. Moudrak. (2–5, Mar.). Interoperability on time: GPS-Galileo offset will bias position. [Online]. GPS World. Available: www.gpsworld.com

[16] E. D. Kaplan and C. J. Hegarty, Eds., *Understanding GPS Principles and Applications*, 2nd ed. Norwood, MA: Artech House, 1996.

[17] Y. Junlin, C. C. Tiberius, P. J. G. Teunissen, G. Bellusci, and G. J. M. Janssen, "A framework for low complexity least-squares localization with high accuracy," *IEEE Trans. Signal Processing*, vol. 58, no. 9, pp. 4836–4847, Sept. 2010.

[18] S. Bancroft, "An algebraic solution of the GPS equations," *IEEE Trans. Aerosp. Electron. Syst.*, vol. 21, no. 1, pp. 56–59, Jan. 1985.

[19] J. B.-Y. Tsui, *Fundamentals of Global Positioning System Receivers. Hoboken*, NJ: Wiley, 2004.

[20] *Global Positioning System Wing, Navstar GPS Space Segment/User Segment L1C Interfaces, IS-GPS-800, Global Positioning System Wing*, Feb. 2008.

[21] *European Union, European GNSS (Galileo) Open Service Signal in Space Interface Control Document (OS SIS ICD), EU*, Feb. 2010.

[22] F. M. Gardner, *Phaselock Techniques*, 3rd ed. Hoboken, NJ: Wiley, 2005.

[23] R. D. Gaudenzi, M. Luise, and R. Viola, "A digital chip timing recovery loop for band-limited direct-sequence spread-spectrum signals," *IEEE Trans. Commun.*, vol. 41, no. 11, pp. 1760–1769, Nov. 1993.

[24] J. W. Betz and K. R. Kolodziejski, "Extended theory of early-late code tracking for a bandlimited GPS receiver," *J. Inst. Navig.*, vol. 47, no. 3, pp. 211–226, 2000.

[25] F. Pérez-Fontán, B. Sanmartín, A. Steingass, A. Lehner, J. Selva, E. Kubista, and B. Arbesser-Rastburg, "A high resolution model for the satellite-to-indoor channel," in *Proc. Position Location and Navigation Symposium (PLANS)*, 2004, pp. 674–683.

[26] W. C. Stone, "Electromagnetic signal attenuation in construction materials," *NIST, Gaithersburg*, MD., Tech. Rep. 6055, 1997.

[27] S. M. Kay, *Fundamentals of Statistical Signal Processing. Detection Theory*, vol. II. Upper Saddle River, NJ: Prentice-Hall, 1998.

[28] G. López-Risueño and G. Seco-Granados, "C/N0 estimation and near-far mitigation for GNSS indoor receivers," in *Proc. IEEE Vehicular Technology Conf. (VTC)*, June 2005, vol. 4, pp. 2624–2628.

[29] A. Goldsmith, *Wireless Communications*. Cambridge, U.K.: Cambridge Univ. Press, 2006.

[30] C. Macabiau, B. Roturier, A. Benhallam, E. Chatre, "Performance of GPS receivers with more than one multipath," *Proc. Institute of Navigation (ION-GPS)*, 1999, pp. 281–288.

[31] G. L. Turin, "Introduction to spread-spectrum antimultipath techniques and their application to urban digital radio," *Proc. IEEE*, vol. 68, no. 3, pp. 328–353, Mar. 1980.

[32] C. Ma, G.-I. Lee, G. MacGougan, and G. Lachapelle, "GPS signal degradation modelling," in *Proc. Institute of Navigation (ION-GPS)*, 2001, pp. 882–893.

[33] F. Pérez-Fontán, V. Hovinen, E. Kubista, R. Wack, M. Schonhuber, and R. Prieto-Cerdeira, "Characterization of the satellite-to-indoor channel at S-band," in *Proc. EuCAP*, Nov. 2007, pp. 1–7.

[34] G. Hein, M. Paonni, V. Kropp, and A. Teuber, "GNSS indoors. Fighting the fading: Part I," *Inside GNSS*, vol. Mar./Apr., pp. 43–52, 2008.

[35] P. Boulton, A. Read, G. McGougan, R. Klukas, E. Cannon, and G. Lachapelle, "Proposed models and methodologies for verification testing of AGPS-equiped cellular mobile phones in the laboratory," in *Proc. Institute of Navigation (ION-GPS)*, 2002, pp. 200–212.

[36] G. Lachapelle, E. Cannon, R. Klukas, S. Singh, R. Watson, P. Boulton, A. Read, and K. Jones, "Hardware simulator models and methodologies for controlled indoor performance assessment of high sensitivity agps receivers," in *Proc. European GNSS*, 2003, pp. 1–18.

[37] T. Hu, G. Lachapelle, and R. Klukas, "Controlled GPS signal simulation for indoors," *Royal Inst. Navig.*, vol. 60, no. 2, pp. 265–280 2007.

[38] Spirent, SimGEN User Manual—Software for the Spirent Range of Satellite Navigation Simulators, DGP00686AAA, 2004.

[39] R. Watson, G. Lachapelle, R. Klukas, S. Turunen, S. Pietil, and I. Halivaara, "Investigating GPS signals indoors with extreme high-sensitivity detection techniques," *J. Inst. Navig.*, vol. 52, no. 4, pp. 199–213, 2005.

[40] S. Knappe, "Emerging topics: MEMS atomic clocks," in *Comprehensive Microsystems*, vol. 3, Y. Gianchandani, O. Tabata, and H. Zappe, Eds. New York: Elsevier, 2007, pp. 571–612.

[41] R. Lutwak, A. Rashed, D. K. Serkland, G. M. Peake, M. Varghese, G. Tepolt, J. R. Leblanc, and M. Mescher, "The miniature atomic clock. pre-production results," in *Proc. European Frequency and Time Forum*, 2007, pp. 1327–1333.

[42] D. W. Allan, "Time and frequency (time-domain) characterization, estimation, and prediction of precision clocks and oscillators," *IEEE Trans. Ultrason., Ferroelect., Freq. Contr.*, vol. 34, no. 6, pp. 647–654, Nov. 1987.

[43] G. Hein, T. Pany, S. Wallner, and J.-H. Won, "Platforms for a future GNSS receiver," *Inside GNSS*, pp. 56–62, Mar. 2006.

[44] W. Ballantyne, G. B. Turetzky, G. Slimak, and J. Shewfelt. (2006, July). "Powerdown: achieving low energy-per-fix in cell phones," GPS World. [Online]. Available: www.gpsworld.com

[45] H. V. Sorensen and C. S. Burrus, "Efficient computation of the DFT with only a subset of input or output points," *IEEE Trans. Signal Processing*, vol. 41, no. 3, pp. 1184–1200, 1993.

[46] D. Jiménez, G. López-Risueño, G. Seco-Granados, and A. García, "Innovative techniques for GPS indoor positioning using snapshot receiver," in *Proc. Institute of Navigation (ION)*, 2006, pp. 2944–2955.

[47] C. Yang, "Zoom, pruning and partial FFT for GPS signal tracking," in *Proc. Institute of Navigation (ION-NTM)*, 2001, pp. 839–849.

[48] M. Anghileri, M. Paonni, S. Wallner, J.-A. Avila-Rodriguez, and B. Eissfeller, "Ready to navigate. A methodology for the estimation of the time-to-first-fix," *Inside GNSS*, pp. 47–56, Mar./Apr. 2010.

[49] A. Schmid and A. Neubauer, "Differential correlation for Galileo/GPS receivers," in *Proc. IEEE Int. Conf. Acoustics, Speech and Signal Processing (ICASSP)*, 2005, pp. 953–956.

[50] M. L. Psiaki, "Block acquisition of weak GPS signals in a software receiver," in *Proc. Institute of Navigation (ION-GPS)*, 2001, pp. 2838–2850.

[51] N. I. Ziedan, *GNSS Receivers for Weak Signals*. Norwood, MA: Artech House, 2006.

[52] F. V. Diggelen, *A-GPS: Assisted GPS, GNSS and SBAS*. Norwood, MA: Artech House, 2009.

[53] D. Borio, M. Fantino, and L. Lo Presti, "The impact of the Galileo signal in space in the acquisition system," in *Proc. Tyrrhenian Int. Workshop Digital Communications*, 2006, pp. 151–167.

[54] L. Vittorini and B. Robinson, "Frequency standards: Key enablers to optimize indoor GPS performance," in *Proc. Institute of Navigation (ION-GPS/GNSS)*, 2003, pp. 660–678.

[55] D. M. Lin and J. B. Y. Tsui, "Acquisition schemes for software GPS receivers," in *Proc. Institute of Navigation (ION-GPS)*, 1998, pp. 317–325.

[56] D. M. Lin and J. B. Y. Tsui, "Comparison of acquisition methods for software GPS receivers," in *Proc. Institute of Navigation (ION-GPS)*, 2000, pp. 2385–2390.

[57] G. López-Risueño and G. Seco-Granados, "Measurement and processing of indoor GPS signals using one-shot software receiver," in *Proc. ESA Navitec Conf.*, 2004, pp. 1–9.

[58] G. W. Heckler and J. L. Garrison, "Experimental tests of unaided signal acquisition methods using a software receiver," in *Proc. Institute of Navigation (ION)*, 2006, pp. 1309–1320.

[59] L. Lo Presti, Z. Xuefen, M. Fantino, and P. Mulassano, "GNSS signal acquisition in the presence of sign transition," *IEEE J. Select. Topics Signal Processing*, vol. 3, no. 4, pp. 557–570, Aug. 2009.

[60] R. E. Blahut, *Fast Algorithms for Digital Signal Processing*. Reading, MA: Addison-Wesley, 1985.

[61] M. Toledo, Y. Capelle, G. Seco-Granados, A. Mark, I. Fernández, D. Kubrak, M. Monnerat, J. A. López-Salcedo, and J. L. Vicario, "DINGPOS: Indoor navigation demonstration platform," in *Proc. European Navigation Conf. (ENC-GNSS)*, Toulouse, France, Apr. 2008, pp. 1–12.

[62] G. López-Risueño and G. Seco-Granados, "Detection and mitigation of cross-correlation interference in high-sensitivity GNSS receivers," in *Proc. IEEE Int. Symp. Personal, Indoor and Mobile Radio Communication (PIMRC)*, Sept. 2007, pp. 1–5.

[63] P. Mattos, "Solutions to the cross correlation and oscillator stability problems for indoor C/A code GPS," in *Proc. Institute of Navigation (ION), Portland, OR*, Sept. 9–12, 2003, pp. 654–659.

[64] P. H. Madhani, P. Axelrad, K. Krumvieda, and J. Thomas, "Application of successive interference cancellation to the GPS pseudolite near-far problem," *IEEE Trans. Aerosp. Electron. Syst.*, vol. 39, no. 2, pp. 481–488, Apr. 2003.

[65] M. Latva-aho and J. Lilleberg, "Parallel interference cancellation. A multiuser detection framework," in *Proc. Symp. Interference Rejection and Signal Separation in Wireless Communications (IRSS)*, Newark, NJ, 1996, pp. 127–146.

[66] Y. T. Morton, M. Miller, J. Tsui, D. Lin, and Q. Zhou, "GPS civil signal self-interference mitigation during weak signal acquisition," *IEEE Trans. Signal Processing*, vol. 55, no. 12, pp. 5859–5863, Dec. 2007.

[67] J. W. Betz, "Effect of partial-band interference on receiver estimation of C/N0: Theory," in *Proc. ION Nat. Tech. Meeting*, 2001, pp. 817–828.

[68] G. López-Risueño, G. Seco-Granados, and A. García, "Evaluation of GPS indoor positioning using real measurements and one-shot software receiver," in *Proc. European Navigation Conf. GNSS*, July 2005, pp. 1–9.

[69] E. Falletti, M. Pini, L. Lo Presti, and D. Margaria, "Assessment of low complexity C/N0 estimators based on M-PSK signal model for GNSS receivers," in *Proc. IEEE/ION Position, Location and Navigation Symp. (PLANS)*, 2008, pp. 167–172.

[70] N. Sirola and J. Syrjarinne, "GPS position can be computed without the navigation message," in *Proc. Institute of Navigation (ION-GPS)*, 2002, pp. 2741–2744.

[71] B. Peterson, R. Hartnett, and G. Ottman, "GPS receivers structures for the urban canyon," in *Proc. Institute of Navigation (ION-GPS)*, Palm Springs, CA, Sept. 12–15, 1995, pp. 1323–1332.

[72] D. Jiménez-Banos, "Enhanced techniques for indoor positioning GPS receivers," European Space Agency (ESA), European Space Research and Technology Center (ESTEC), Noordwijk, The Netherlands, *ESA Rep.*, 2006.

[73] A. Angrisano, S. Gaglione, A. Pacifico, and M. Vultaggio, "Multi-constellation system as augmentation to GPS performance in difficult environment or critical application," in *Proc. European Navigation Conf. (ENC-GNSS)*, 2009, pp. 1–10.

[74] T. Pany, B. Riedl, and J. Winkel, "Efficient GNSS signal acquisition with massive parallel algorithms using GPUs," in *Proc. Institute of Navigation (ION-GNSS)*, Portland, OR, Sept. 21–24, 2010, pp. 1889–1895.

[75] G. Hein, A. Teuber, H.-J. Thierfelder, and A. Wolfe, "GNSS indoors. Fighting the fading: Part II," *Inside GNSS*, vol. May/June, pp. 47–53, 2008.

[76] G. Hein and A. Teuber, "GNSS indoors. Fighting the fading: Part III," *Inside GNSS*, vol. July/Aug., pp. 45–53, 2008. [SP]